

We wish to thank the reviewers for their comments that have substantially improved our manuscript. We feel that we have addressed all major and minor comments that were raised by the reviewers and, in doing so, have crafted a revised manuscript that is more rigorous in content, and better shows the connection of the various aspects of large scale circulation and air pollution changes. In doing so, we have not structurally changed the manuscript but we have substantially modified section 3 and added 3 appendixes (A, B and C), providing more in-depth discussions on NAOI-Coherence Index and blocking frequency relationship (Sects. 3.1 and 3.2, appendix A). We have also inserted a discussion on the relationship of circulation changes and precipitation for the 2000 simulation (appendix B) together with an analysis of precipitation change in the 2030 sensitivity experiments (appendix C).

Here below, we copy the comments/concerns (in bold) and describe how each of these issues has been addressed in the revised manuscript. The revised version of the manuscript is attached after the answers to reviewers' comments, and the changes compared to the ACPD version are highlighted in bold italic.

Reviewer #1

Reviewer #1 major concern was the lack of a clear connection between the different aspects presented in the paper: the impact of aerosols on the NAO, the impact of aerosols on the coherence index over the Atlantic basin, the impact of aerosols on changes in blocking and on changes in the local pollutant distribution over Europe. He/she felt the link was not clearly demonstrated. We have already partially addressed this concern in the previous answer (acpd-14-C7882-2014.pdf); here, we expand it answering to each specific comment and pointing out how we have implemented it in the revised manuscript.

Major Comments

1) “**The paper shows that shape of the aerosol distribution changes over Europe depending on the aerosol forcing. In some regions the skewness of the distribution is increased, in others it decreases. The paper goes on to attribute these differences to changes in blocking. I really do not see any convincing demonstration that this is indeed the case. While changes in blocking may impact aerosol distributions there could be a multitude of reasons for the change in shape of the simulated aerosol distributions. This change may or may not be directly related to changes in blocking. For example changes in the mean precipitation, changes in the structure of the boundary layer etc may be responsible for the change in the skewness of the aerosol distribution. For this paper to work the authors need to show the changes in the aerosol distribution can be attributed to changes in blocking. (Indeed it would appear that the situation is slightly more complicated than can be explained by changes in blocking alone. Although it is somewhat difficult to say, it appears the changes in the aerosol distributions do not directly correlate with the changes in the blocking. For example, the 2030AER simulation appears to have less change in blocking than the 2000MFR simulation in the Western Mediterranean region, but approximately the same change in skewness.)**”

Thank you for pointing this out. The relationship between the changes in atmospheric

blocking and the changes in aerosol distribution were indeed not sufficiently clearly discussed.

As we mentioned in the preliminary reply (acpd-14-C7882-2014.pdf), we agree with the reviewer that also other factors – such as changes in the mean precipitation or the structure of the boundary layer – could influence the change in shape of the simulated aerosol distributions. However, we argue that these factors are implicitly included in our analysis, since changes in the Coherence Index (CI), NAOI and blocking events impact many parameters associated with atmospheric circulation, including precipitation amounts/distributions/frequencies and as well as the structure of the boundary layer. Hence, we consider the latter to be the more localized expressions of the large-scale circulation pattern changes, which are the subject of our paper. In a previous paper, using the same modeling framework in a re-analysis set-up, Pausata et al. (2013) already demonstrated the significant link between PM and NAOI in winter under past (1990–2005) conditions (Fig. 2 in Pausata et al. 2013): a more positive NAOI leads to more stable conditions over central–western Mediterranean basin as shown in figure R1 and consequently increased positive PM anomalies. To further explain some of the PM distribution changes under climate change conditions in our study we have now also included further analysis following the publication by Sillmann et al. (2013), who have used the same model and simulation set-up to investigate changes in extreme events in the future focusing on annual means. We now discuss in Section 3.3 and Appendix B our PM distribution changes taking into account not only the large-scale atmospheric circulation changes, but also future changes in the frequency of rainy-day that can affect aerosol distributions. We also discuss in appendix B the relationship between atmospheric circulation (specifically NAOI and CI shifts) and the frequency of rainy-days (in our model defined as grid cells with PRECT>1 mm/day). As expected the changes in rainy-day are strongly linked to the phase of the NAO or the position of the SLP centres of actions (see appendix B in the revised manuscript).

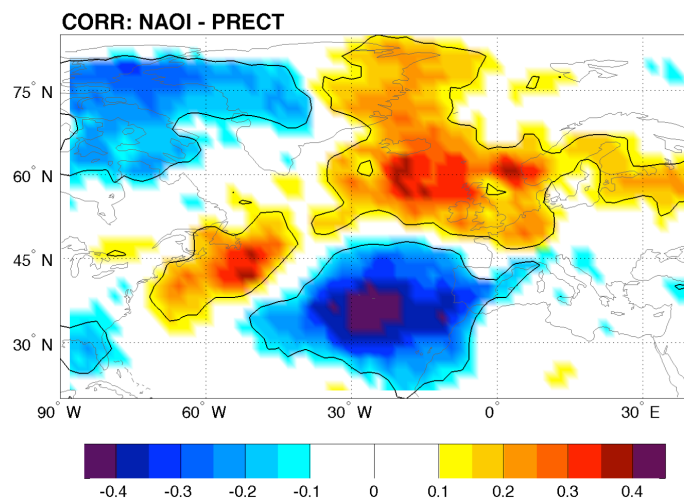


Figure R1: Correlation between NAOI and monthly precipitation amounts. The contours indicate the significant areas at 95% confidence level.

Finally, we feel the reviewer perhaps had a somewhat different expectation regarding the aim of the paper. Our goal was not per-se to demonstrate a change in aerosol distribution due to changes in blocking frequency. Rather our main goal was to demonstrate the different roles of the aerosol and GHG in affecting atmospheric circulation and hence on potential repercussions on air-quality. Although changes in blocking frequency (BF) was one way to look at circulation changes, other atmospheric circulation change indicators (NAOI, CI) are equally useful to demonstrate an increase in extreme pollution events over Western Mediterranean.

2) The paper suggests that changes in blocking over Europe can be attributed to changes in the NAO. If I understand the paper correctly, the scientific literature suggests that changes in high latitude blocking are associated with changes in the NAO, but it is not clear to me how changes in lower latitude blocking over Europe relate to the NAO. The authors need to conclusively show that the changes in the NAO are associated with the changes in lower latitude blocking over Europe.

The NAO is connected to both high latitude and low latitude blockings (for more details see ‘Preliminary answer to Reviewer #1’). We have integrated this discussion in Section 3.2. We have also included in the manuscript a new figure (new Figure 4 panel a) showing the regression of the NAOI onto the BF field. The regression analysis shows the explained amount of BF change per NAOI=1 for more details see Appendix B in the manuscript. During positive phases of the NAO, the number of high latitude blocking events decreases (deeper Icelandic low) whereas the LLB increases especially over the southern North Atlantic (stronger Azores/sub tropical High) – see figure 4 in the revised manuscript.

A relationship between positive NAO phases and increased blocking frequency over Europe has been also described in details by e.g. Yao and Luo (2014), in this sense our paper confirms a wider body of literature evidence.

3) The relationship between the coherence index, the NAO and blocking over Europe is not clear to me. Are the authors claiming that shifts in the coherence index are related to shifts in the NAO? Can the authors prove this? How do shifts in the coherence index relate to blocking? These links need to be shown statistically and conclusively in the paper.

What we do in this manuscript is using a climate model with identical physical description of physical and chemical processes, and change a limited set of the boundary conditions (i.e. GHG concentrations, and aerosol abundances). The ‘prove’ of relationships between various circulation responses, is then given by showing spatial correlation structures, which are significant at certain probability levels. This is common approach in geo-statistics, but it should also be recognized that following this approach that there is always a remaining possibility that processes are not related (despite a high correlation). To demonstrate the link between CI and NAOI, we have calculated the correlation between SLP and leading Principal Component

(PC) of the SLP field following Pausata et al. 2009 study (for more details see ‘Preliminary answer to Reviewer #1’). For simplicity, in the manuscript and later on in the reply, we have used the canonical definition of the NAOI, since PC1 and NAOI in winter are highly correlated ($r > 0.90$, see also Hurrell, 1995).

Figure R2 shows that the correlation between PC1 and SLP is very similar to the CI pattern and the correlation maxima of both analyses are quite close to each other. The advantage of the CI analysis compared to the PC/SLP (or temperature or precipitation) correlation analysis is that the CI analysis does not depend only on the leading mode of variability but directly integrates all other modes that directly affect the fluctuations of the analyzed variable.

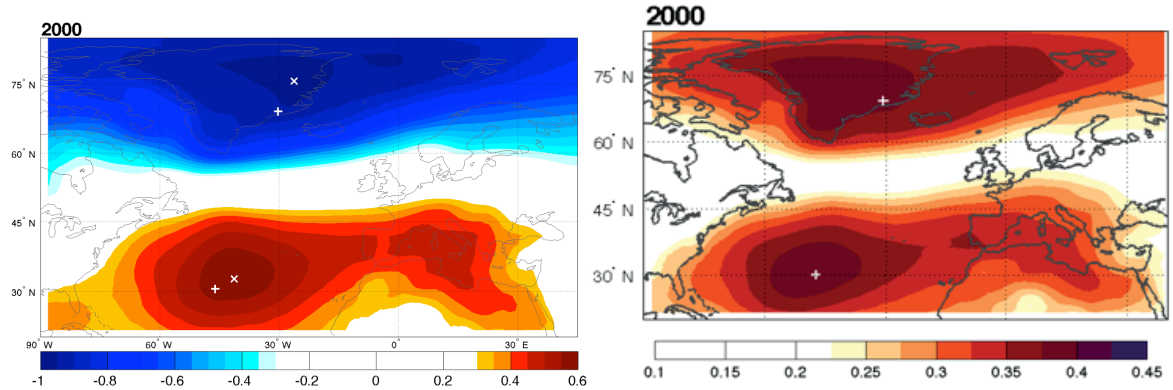


Figure R2: Correlations between North Atlantic winter SLP (December to February) and PC1 of SLP (left) and coherence index of winter SLP (right). The markers indicate the maxima in CI (+ sign) and in the SLP/PC1 (x sign) correlation.

Pausata et al. (2009) have shown that, while in present day climate the CI and PC correlations are very similar, during different climate states they can be completely different (Figures 7 and 8 in Pausata et al., 2009).

We have therefore decided to adopt the CI as a further variability metric in addition to the canonical NAOI to better understand and interpret large-scale circulation changes: while the NAOI gives a good picture of some features of the mid-latitude atmospheric circulation (strength and direction of the westerly mid-latitude flow), the CI provides additional information on atmospheric variability at a domain scale, specifically the shifts in the centers of action.

We have included a discussion about the relationship between NAOI and CI on an Appendix to the manuscript (Appendix A).

To show the relationship between CI maxima and BF we need to construct an index based on the position of the southern SLP center of action (SCOAI) and investigate its link to the frequency of blocking events. We have used 10000 random subsamples of 15 years taken from the 60-year pool of the 2000 simulation and generated via bootstrapping. SCOAI equal 0 is defined as the 50th percentile — calculated using the 10000 subsamples — of the southern SCOAI position. Eastward positions (relative to the 50th percentile) of the southern SCOAI are defined as positive values and westward position as negative values of the SCOAI. The SCOAI has then been normalized by

the standard deviation of the SCOAI positions. We have then calculated a correlation (Fig. R4) between SCOAI and BF (calculated considering the same years consider when constructing the SCOAI) and performed a regression analysis (Fig. 4 panel b in the manuscript).

We have included a discussion about the relationship between NAOI and CI on an Appendix to the manuscript (Appendix A).

We have included a discussion about the relationship between SCOAI and BF in the manuscript (see discussion on figure 4).

4) The authors seem to want to make the broad claim that changes in the aerosol emissions are primarily causing shifts in the NAO index and in the coherence index. The case for this seems to me to be somewhat shaky. If the authors are not making this claim they need to clearly state the features for which they believe the role of aerosol forcing is most dominant (versus the forcing due to GHGs), and for which features they can not make a clear determination.

(i) If I understand the paper correctly, neither changes in GHG or in aerosols alone can be shown to statistically result in the shift in the NAO. It is only the combination of both these forcings that results in the shift in the NAO. Therefore, it is difficult to attribute difference in the NAO predominantly to differences to aerosol forcing.

Thanks for pointing it out. We did not mean to say that shifts in NAO are due predominantly to aerosol, but rather the shift in the southern SLP center of action is mainly due to the aerosol forcing. We believe we have now made it clear in the manuscript rewriting the following paragraph at the end of section 3.1:

“With regard to the SLP variability, the 2030 simulation shows a significant positive shift of the NAO mean state of 0.46 compared to the 2000 control period (Fig. 2). The probability of having an NAOI greater than +1 increases from 30% to 40% (Fig. 2). Neither the GHG increase (2030GHG) nor the aerosol reduction (2030AER) have statistically significant role in changing the NAO mean state and the frequency distribution of strongly positive/negative NAO phases relative to the control simulation. Nevertheless, the GHG increase seems to provide a stronger contribution to the NAO shift; the 2030AER NAO shift is significant at the 65% confidence level, while the 2030GHG one at the 85% level (using a t-test). Only the combination of both 2030 GHGs and aerosol emissions leads to a statistically significant change in the NAO mean state at 95% confidence level.

Hence, whereas the NAO shift is related to both aerosol and GHG changes (with likely stronger impacts from the GHGs), the aerosol reduction alone plays the largest role in shifting the southern centre of action of SLP towards the Mediterranean.”

(ii) Both the 2030GHG and the 2030AER simulations stretch the coherence index towards Southern Europe. Although the 2030AER distribution “looks” somewhat more like the 2030MFR distribution (thus suggesting the final distribution is forced more by the aerosols than GHGs) it is somewhat unclear that this is really statistically significant.

We have now included in figure 1 the 10th and 90th percentile of the positions of the maxima for the 2000 simulation. It has been calculated generating 100 subsamples of 40 years (via bootstrap technique) and calculating the CI maxima. This analysis confirms indeed that aerosol changes are the primary driver of southern CI maxima.

We have also generated 100 subsamples of 20 years for the other simulations and then calculated the t-test between the 2000 simulation and all the other experiments to evaluate whether there were significant differences in the CI pattern. In figure 1 in the manuscript only significantly different values are shown. Most of the change in the CI pattern are significant at 95% confidence level for all sensitivity experiments relative to the 2000 control.

5) The authors should show the difference in the radiative forcing for both aerosols and greenhouse gases between 2030 and 2000.

The differences in radiative forcing for all simulations used in our analysis have been already reported in Table 2 in Kloster et al. (2009), reported here below.

Table 2 Total sky top-of-the-atmosphere (TOA), surface and atmosphere net (shortwave plus longwave) radiative forcing (RF) in W m⁻² as simulated in Kloster et al. (2008)

	TOA			Surface			Atmosphere		
	Global	NH	SH	Global	NH	SH	Global	NH	SH
<i>GHG+AE</i>	2.66	3.30	2.03	2.21	2.99	1.45	0.45	0.31	0.58
<i>GHG+DT</i>	1.71	1.82	1.58	1.10	1.27	0.95	0.60	0.55	0.63
<i>GHG+IP</i>	2.24	2.70	1.79	1.64	2.07	1.22	0.61	0.63	0.58
<i>GHG</i>	1.53	1.53	1.54	0.84	0.81	0.88	0.69	0.72	0.66
<i>AE</i>	1.13	1.77	0.49	1.37	2.18	0.57	-0.24	-0.41	-0.08

RF is here defined as the difference between the perturbed future simulations minus the present day (2000) simulation. Atmospheric RF is calculated as the difference in net radiation between TOA and surface

We would like to point out that the spatial distribution of the radiative forcing is in general uncorrelated with surface climate (e.g., surface temperature or SLP) as shown for example in Lewinschal et al., (2012).

6) Is Figure 4 based on monthly mean values (as implied in the figure caption)? This figure really should be based on daily maximum values. Air pollution regulations are based on daily values, as the authors are aware. If they based their statistics on monthly values this needs to be clearly stated and rationalized.

We agree with the reviewer #1 that for policy regulations daily data should be analyzed. Unfortunately, moving model datasets between computer systems (the simulations were done few years ago), the computed hourly and daily concentration datasets were erroneously deleted. While this is a major drawback, we are certain that a fair amount of the changes in daily maximum values, are reflected in monthly changes as well. We also realized that our coarse resolution dataset, would only have limited skills in representing daily maximum concentrations, meaning that inaccuracies in this parameter would have been distracting from the research question: “the coherence of large-scale circulation changes on air-quality”. Finally, long-term regional climate models driven by global boundary conditions should be explored to look into this issue rather than global models.

We have add the following sentence to clarify this aspect:

"We aim at providing a general coherent overview of the impacts of large-scale circulation changes on air-quality. We focus on monthly PM data, similar to the monthly SLP field used for the NAOI and CI analyses. We do not discuss the daily exceedances of EU thresholds, since this would be beyond the scope of the present study and the coarse resolution global model has limited skills on simulating them (Pausata et al., 2013)."

Minor Comments

– P22481, l18–19 extension → extent Is this a reduction to the maximum feasible extent of aerosol emissions everywhere or just over Europe?

It's globally, we have specified it in the text. Now it reads:

We focus on the extreme case that by 2030 aerosol concentrations will be globally reduced to the maximum feasible extent by using all presently available end-of-pipe technology.

– P22481, l22–23: While in the first sentence here the authors state aerosol emissions change between simulations in the 2nd sentence they state that the emission scenarios used to force the model are constant. Please clarify.

Thank you for pointing it out. We have rephrased it as follow:

The analysis includes simulations in which only GHG concentrations, only aerosol emissions or both are changed. In each simulation the anthropogenic emission scenarios used to force the model are constant for the entire length of the integration; hence, the changes in variability depicted by the model will be associated with changes in atmospheric circulation only.

– P22482–22483: Please state whether the model setup includes a simulation of the indirect effects?

Yes it does include it and we have now made it clear in the text. Now it reads:

The ECHAM5-HAM modeling system includes the atmospheric general circulation model ECHAM5 (Roeckner et al., 2003) coupled to a mixed layer ocean (Roeckner et al., 1995), and the microphysical aerosol model HAM (Stier et al., 2005). The ECHAM5-HAM simulations analysed in this study (Kloster et al., 2008, 2009) account for both the direct and indirect (cloud lifetime and cloud albedo effect) aerosol effects.

– P22484: Are these simulations in climate equilibrium?

Yes they are at the equilibrium as reported in L 1 pag. 22484. We have further clarified it, specifying in the text that all simulations are at the equilibrium.

- P22484, l7–12: It might be clearer here if you listed all experiments together instead of omitting the control experiment.

Thank you, we have included the 2000 simulation description as well.

- P22484: I find the names of the experiments somewhat confusing. 2030MFR refers to the simulation where both GHG and aerosol were set to 2030 levels, while 2030AER also uses 2030 MFR aerosols, but 2000 GHGs. Maybe 2030MFR should be referred to simply as 2030?

Thanks for the suggestion. Hence, we decided to use the label ‘2030’ instead of ‘2030MFR’.

- Figure 1 and discussion on the coherence maps. The statistical significance of these changes in the coherence is unclear to me. The authors need to make clear the changes that are significant.

We have included the significance in the revised version of figure 1 (see also answer to major comment #4ii)

- I find Figure 2 somewhat misleading. The control experiment is 60 years, the others 30 years. While this makes plotting easier it makes it more difficult to compare the distributions. The authors should probably normalize these plots to the same number of years or make them frequency plots to facilitate better comparisons.

Thank you. We follow the reviewer suggestion normalizing the experiments. We have scaled accordingly the 2000 simulation (see new figure 2 in the revised manuscript).

- P22487,l16–18 This statement is really not accurate as stated. A more accurate statement would be “Neither the 2030GHG or the 2030AER play a statistically significant role in changing the NAO state.... “. If I understand the authors here neither the 2030GHG or the 2030AER simulations are statistically different than the control simulation.

As the reviewer pointed out neither GHG nor AER alone are able to change significantly the NAO, so in that sense they play a similar role. We wanted to highlight the fact that anyway both of them do lead to a small shift of the NAO that is not significant at 95% confidence level, but it is at a lower level (85% for AER and 80% for GHG). Given that the sum of the GHG and AER does lead to a significant shift, it’s unlikely that the shift seen in GHG and AER simulation is positive by chance.

We have rephrased that sentence as follow:

Neither the GHG increase (2030GHG) nor the aerosol reduction (2030AER) have statistically significant role in changing the NAO mean state and the frequency distribution of strongly positive/negative NAO phases relative to the control simulation. Nevertheless, the GHG increase seems to provide a stronger contribution to the NAO shift; the 2030AER NAO shift is significant at the 65% confidence level,

while the 2030GHG one at the 85% level (using a t-test). Only the combination of both 2030 GHGs and aerosol emissions leads to a statistically significant change in the NAO mean state at 95% confidence level.

– P22487, l20–21. This statement is only technically accurate: “In conclusion, whereas both GHG and aerosol changes have similar impacts on the NAOI frequency shift.” They are both similar because neither of them is statistically significant.

The reviewer is indeed correct, but what we meant is that “even though neither the 2030GHG or the 2030AER play a statistically significant role in changing the NAO state when considered alone, when considered together they lead to a NAO shift”, so in that sense “Both GHG and aerosol changes have similar impacts on NAOI frequency. We have rephrased it and now it reads:

Hence, whereas the NAO shift is related to both aerosol and GHG changes (with likely stronger impacts from the GHGs), the aerosol reduction alone plays the largest role in shifting the southern centre of action of SLP towards the Mediterranean.

– Figure 3. Blocking frequency is given in percent, but percent of what? Percent of time during the winter months a block occurs at any gridpoint?

Thanks for pointing this out. We have included a better description in the figure caption. The percent refers to the percentage of days in which there is a blocking event. Now it reads:

Blocking frequency (in % of days in which a blocking event occurs at a given grid box) over the Atlantic sector for the 2000 simulation (a);...

– Table 2 states all changes are significant at the 95% level. Is this change from the control? (The text implies not, but the figure caption should be clarified)

We have clarified in the table caption, now it reads:

Skewness values for the PM distributions of the four selected regions for each experiment. For each region and experiment, changes relative to all the other experiments are significant at the 95% confidence level, except for 2030-2030AER in Western Mediterranean.

– Figure 3. Can you mark the regions evaluated in Table 2 in Figure 3?

We have highlighted the regions in the revised version of Figure 3 panel a. Here below we reported it (Fig. R3)

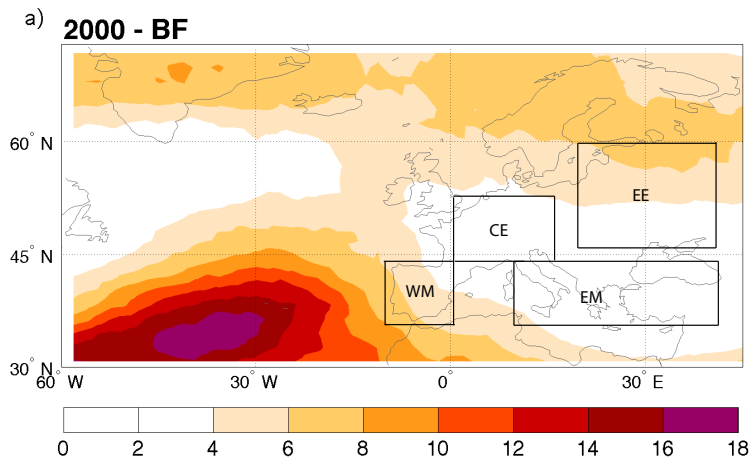


Figure R3: Blocking frequency (in % of days in which a blocking event occur at a given grid box) over the Atlantic sector for the 2000 simulation. The regions discussed in Section 3.3 and Table 2 are highlighted.

- P22490, l4. “Extreme” doesn’t really belong here. Skewness implies positive values are more likely than negative values.

Thanks, we have modified the text accordingly, removing “extreme”.

Reviewer #2

The Reviewer #2 had the same main concerns as Reviewer #1, in addition he/she highlighted some minor issues that have been addressed as described below.

- In addition to reviewer #1 replies, I would like to see a figure/sketch that summarizes the findings of the study in terms of shifts/extensions of SLP centers and blockings.

We have added Table R1 in the revised manuscript as Table 4.

Table R1: Qualitative contributions (small (+), medium (++) , high (+++)) of 2030 GHG and AER to changes in the NAO phase, SCOA location and blocking event frequency. For the blocking events the direction of the increased frequency is also shown. The contributions significant at 95% confidence level are shown in bold

	Impact on NAO	Impact on SCOA	Impact on Blocking Events
2030GHG	++	+	North ++ East +
2030AER	+	+++	North ++ East +++
2030 (GHG+AER)	+++	+++	North +++ East +++

- Also it would have been very useful to the reader to see on a map (can be in one of the existing figures) the four regions that are analyzed for air quality impacts, regions for which the longitudes and latitudes are provided in p22489 l15–18. In addition, there, please check the boarders – for instance EM does not

extend to 40W, the authors might mean 40E. Can the authors explain why the specific boundaries have been chosen for these 4 regions? Why the ‘central Mediterranean’ is left out or the south Mediterranean Sea/North Africa is not part of the Mediterranean regions.

Thank you, indeed for EM 40°E was intended. We have included the analyzed regions in the revised Figure 3 panel a (Fig. R4). In the choice of the 4 domains we have focused over Europe and tried to include the most populated areas. The Central Mediterranean countries are therefore included and belong to the EM region.

- **P 22490, l 27: Could it be that the long-range transport pollution source region is differently affected in the Western than in the Eastern Mediterranean?**

It may well be, anyway in lights of the new analysis we have slightly modified that paragraph and now it reads:

The Eastern Mediterranean (EM) also experiences an increased skewness in the 2030 simulation relative to 2000. However, the changes are smaller compared to the WM, possibly because of the greater distance from the SCOA – located off the coast of the Iberian Peninsula in 2030 simulation – and the contrasting effect of the NAO phase inside the domain (Fig. B1a): as one moves further to the east in the Mediterranean basin, the correlation between NAO and precipitation changes sign (Fig. B1a). The smaller changes in the PM distribution simulated in EM compared to WM could therefore be related to a different behaviour in precipitation regime (see Appendix B).

- **P 22488, l19–22: Is this finding statistically significant for 2030AER?**

It is indeed significant as shown in figure 3 (shading are the area with significant changes) in the ACPD manuscript. We have rephrased the paragraph. See comment below.

- **P 22488, l221–22: this statement requires supporting evidence.**

We have rephrased the paragraph as follow:

The 2030GHG and 2030AER simulations also show significant increases in the frequency of LLB events over the mid-latitude North Atlantic and decreases in the frequency of HLB (Fig. 3c and 3d). However, the patterns are different from one another: the high-latitude change in both 2030GHG and 2030 closely approximates the blocking frequency difference between the positive and negative phases of the NAO shown in figure 4a (cf. with figure 3b and 3c). On the other hand, the HLB frequency change in the 2030AER experiment seems to be related to a shift in the SCOA (cf. 3d and 4b). This is would be in agreement with the large (small) eastward displacement of the SCOA in the 2030AER (2030GHG) simulation and the smaller (larger) shift in the NAO mean state.

- **P 22483, l1–2: Can you provide an estimate on the errors induced in sulfate and more generally PM calculations by the assumption of prescribed oxidant**

fields?

We have added the following sentence:

Prescribing oxidant concentrations, most importantly H_2O_2 , may have led to an underestimate in the resulting sulfate burden, since the use of off-line H_2O_2 may not accurately account for depletion by aqueous reactions with SO_2 and recovery in cloud-free conditions. This will increase the gas-phase production of SO_4 , which is less susceptible to scavenging, and increase the SO_4 burden (Barth et al., 2000; Roelofs et al., 1998). Another model evaluation of the effect of including explicit oxidation (Pham, 2005) suggested an overall decline of SO_4 burden (<1 %), but an increase of SO_4 surface concentrations (ca. 5% in many regions), due to a combination of increased near-surface oxidation and removal processes. This is a relatively minor error compared to other uncertainties (Textor et al., 2007).

– P 22483, l3–5: Provide reference of the model using this module for aerosol radiative properties.

The aerosol radiative properties are pre-calculated using the Mie-Theory. This is actually part of the HAM model and details are given in Stier et al. (2005).

We have added the reference at the end of the following sentence:

The aerosol optical properties were explicitly simulated within the framework of the Mie theory and provided as input for the radiation scheme in ECHAM5, following Toon and Ackerman, (1981).

– P 22484, l12,13: GHG concentrations and aerosol emissions . . . , respectively.

We have rewrote that sentence and now it reads:

The 2030GHG and 2030AER experiments in which, respectively, aerosol emissions and GHG concentrations remained at the 2000 level, were performed to separate the effects of GHG concentrations and aerosols emissions.

– P 22486, l24: show

Thank you. We have modified it.

– P 22492, l3: Hori et al reference is missing.

Thanks for pointing this out. We have now included it.

References

- Barth, M. C., Rasch, P. J., Kiehl, J. T., Benkovitz, C. M. and Schwartz, S. E.: Sulfur chemistry in the National Center for Atmospheric Research Community Climate Model: Description, evaluation, features, and sensitivity to aqueous chemistry, *J. Geophys. Res.*, 105(D1), 1387, doi:10.1029/1999JD900773, 2000.
- Hurrell, J. W.: Decadal trends in the north atlantic oscillation: regional temperatures and precipitation., *Science*, 269(5224), 676–9, doi:10.1126/science.269.5224.676, 1995.
- Kloster, S., Dentener, F., Feichter, J., Raes, F., Lohmann, U., Roeckner, E. and Fischer-Bruns, I.: A GCM study of future climate response to aerosol pollution reductions, *Clim. Dyn.*, 34(7-8), 1177–1194, doi:10.1007/s00382-009-0573-0, 2009.
- Lewinschal, A., Ekman, A. M. L. and Körnich, H.: The role of precipitation in aerosol-induced changes in northern hemisphere wintertime stationary waves, *Clim. Dyn.*, 41(3-4), 647–661, doi:10.1007/s00382-012-1622-7, 2012.
- Pausata, F. S. R., Pozzoli, L., Dingenen, R. Van, Vignati, E., Cavalli, F. and Dentener, F. J.: Impacts of changes in North Atlantic atmospheric circulation on particulate matter and human health in Europe, *Geophys. Res. Lett.*, 40(15), 4074–4080, doi:10.1002/grl.50720, 2013.
- Roelofs, G.-J., Lelieveld, J. and Ganzeveld, L.: Simulation of global sulfate distribution and the influence on effective cloud drop radii with a coupled photochemistry sulfur cycle model, *Tellus B*, 50(3), doi:10.3402/tellusb.v50i3.16098, 1998.
- Sillmann, J., Pozzoli, L., Vignati, E., Kloster, S. and Feichter, J.: Aerosol effect on climate extremes in Europe under different future scenarios, *Geophys. Res. Lett.*, 40(10), 2290–2295, doi:10.1002/grl.50459, 2013.
- Stier, P., Feichter, J., Kinne, S., Kloster, S., Vignati, E., Wilson, J., Ganzeveld, L., Tegen, I., Werner, M., Balkanski, Y., Schulz, M., Boucher, O., Minikin, A. and Petzold, A.: The aerosol-climate model ECHAM5-HAM, *Atmos. Chem. Phys.*, 5(4), 1125–1156, doi:10.5194/acp-5-1125-2005, 2005.
- Toon, O. B. and Ackerman, T. P.: Algorithms for the calculation of scattering by stratified spheres., *Appl. Opt.*, 20(20), 3657–60, doi:10.1364/AO.20.003657, 1981.
- Yao, Y. and Luo, D.: Relationship between zonal position of the North Atlantic Oscillation and Euro-Atlantic blocking events and its possible effect on the weather over Europe, *Sci. China Earth Sci.*, doi:10.1007/s11430-014-4949-6, 2014.

1 **The role of aerosol in altering North Atlantic atmospheric**
2 **circulation in winter and impact on air-quality**

3 Francesco S.R. Pausata^{1,2*}, Marco Gaetani¹⁺, Gabriele Messori², Silvia Kloster³, and Frank J.
4 Dentener¹

5 *Affiliation*

6 ¹*European Commission, Joint Research Centre, Institute for Environment and Sustainability,*
7 *Ispra (VA), Italy*

8 ²*Department of Meteorology, Stockholm University and Bolin Centre for Climate Research,*
9 *Stockholm, Sweden*

10 ³*Land in the Earth System, Max Planck Institute for Meteorology, Hamburg, Germany*

11 *now at *Department of Meteorology, Stockholm University and Bolin Centre for Climate*
12 *Research, 10691, Stockholm, Sweden*

13 +now at *LATMOS-IPSL, Université Pierre et Marie Curie, Paris, France*

14 Corresponding author: francesco.pausata@misu.su.se;

16 Numerical model scenarios of future climate depict a global increase in temperatures and
17 changing precipitation patterns, primarily driven by increasing greenhouse gas (GHG)
18 concentrations. Aerosol particles also play an important role by altering the Earth's radiation budget
19 and consequently surface temperature. Here, we use the general circulation aerosol model
20 ECHAM5-HAM, coupled to a mixed layer ocean model, to investigate the impacts of future air
21 pollution mitigation strategies in Europe on winter atmospheric circulation over the North Atlantic.
22 We analyse the extreme case of a maximum feasible end-of-pipe reduction of aerosols in the near
23 future (2030), in combination with increasing GHG concentrations. Our results show a more
24 positive North Atlantic Oscillation (NAO) mean state by 2030, together with a significant eastward
25 shift of the southern centre of action of sea level pressure (SLP). Moreover, we show a significantly
26 increased blocking frequency over the western Mediterranean.

27 ***By separating the impacts of aerosols and GHGs, our study suggests that future aerosol***
28 ***abatement may be the primary driver of both the eastward shift in the southern SLP centre of***
29 ***action and the increased blocking frequency over the western Mediterranean.*** These concomitant
30 modifications of the atmospheric circulation over the Euro-Atlantic sector lead to more stagnant
31 weather conditions that favour air pollutant accumulation especially in the western Mediterranean
32 sector. Changes in atmospheric circulation should therefore be included in future air pollution
33 mitigation assessments. ***The indicator-based evaluation of atmospheric circulation changes***
34 ***presented in this work will allow an objective first-order assessment of the role of changes in***
35 ***wintertime circulation on future air quality in other climate model simulations.***

36 **1 INTRODUCTION**

37 Future climate scenarios indicate a global increase in temperatures and changes in the
38 hydrological cycle, mainly driven by increasing greenhouse gas (GHG) concentrations (IPCC,
39 2013). However, GHGs are not the only climate factor responsible for changing the Earth's
40 radiation budget. Aerosol particles ("aerosols") also play a very important role in altering climate,
41 both directly – by scattering and absorbing solar radiation – and indirectly – by influencing cloud
42 radiative properties (cloud albedo effect; Twomey, 1977), and cloud formation and duration (cloud
43 lifetime effect; Albrecht, 1989). The direct effect of non-absorbing aerosols – such as sulphates –
44 produces an overall cooling of the atmosphere, while partly absorbing aerosols – such as black and
45 organic carbon – can lead to either a cooling or a warming, depending on the aerosols' properties
46 and underlying albedo.

47 Global climate models can realistically reproduce the temperature trend of the last century only
48 when the radiative impacts of both GHGs and aerosols are included (Gleckler et al., 2008;
49 Nazarenko and Menon, 2005; Roeckner et al., 1999; IPCC 2013). Therefore, increasing GHG
50 concentrations as well as changes in aerosol abundance will control future climate and the
51 associated atmospheric circulation variations. High aerosol concentrations can also have severe
52 impacts on human health (Lim et al., 2012; WHO, 2013). Consequently, air quality standards have
53 been introduced in many polluted regions to regulate harmful aerosol concentrations, and the
54 upward trends in aerosol emissions in the most polluted regions are expected to stabilize or reverse.
55 Hence, a realistic assessment of on-going and future climate change relies on our ability to predict
56 trends in both GHG and aerosol emissions, the resulting concentrations and their combined effect
57 on climate.

58 Most of the GHGs are long-lived and have a geographically homogeneous climate forcing. On
59 the other hand, aerosol concentrations are highly inhomogeneous, since they are locally controlled
60 by a combination of primary or precursor emissions, chemical reactions as well as large-scale
61 atmospheric circulation, and their impacts can have short-term repercussions on climate (Shindell et
62 al., 2012). Furthermore, atmospheric circulation changes themselves can feedback on air quality.
63 Modelling and observational analyses suggest that a warming climate degrades air quality, with
64 increasing surface O₃ and particulate matter abundance in many populated regions (Fiore et al.,
65 2012). Kloster et al. (2009), for example, used a coupled chemistry-atmosphere general circulation
66 model to show that climate change alone would worsen the air pollution by aerosols in many world
67 regions.

68 Several other studies have demonstrated that local-to-regional scale pollutant concentrations
69 can be influenced by large-scale atmospheric circulation patterns (Eckhardt et al., 2003;
70 Christoudias et al., 2012; Barnes and Fiore, 2013; Pausata et al., 2012, 2013), such as the North
71 Atlantic Oscillation (NAO). Pausata et al. (2013) have shown how positive shifts in the NAO in
72 winter over the North Atlantic penalize cities lying in the Mediterranean area, making it necessary
73 for these countries to enforce more stringent emission reduction measures. This is of particular
74 importance in view of a potential shift towards positive NAO regimes under future climate
75 conditions.

76 The NAO commonly refers to swings in the atmospheric pressure difference between the
77 subpolar and subtropical North Atlantic, and is the leading mode of winter atmospheric variability
78 in the North Atlantic. The standard NAO index (NAOI) is defined as the difference in normalized
79 mean sea-level pressure (SLP) between the Azores (or Portugal) and Iceland (Walker and Bliss,
80 1932), and determines climate variability from the eastern seaboard of North America to Siberia
81 and from the Arctic to the subtropical Atlantic. The NAO featured an upward trend of over 1
82 standard deviation in the 1980s and 1990s compared to the 1951–1970 winter mean (data available
83 in <http://www.cgd.ucar.edu/staff/jhurrell/naointro.html>). Recent multi-model predictions confirm
84 previous findings reported in AR4 (e.g., Kuzmina, 2005; Stephenson et al., 2006), of a positive
85 trend in future winter NAO (Gillett and Fyfe, 2013; Karpechko, 2010). However, there are
86 substantial variations between NAO projections from different climate models. For example,
87 Fischer-Bruns et al. (2008) have employed an atmosphere-ocean coupled model (ECHAM4-
88 OPYC3) and used the Empirical Orthogonal Function (EOF) analysis to investigate future trends in
89 the NAO. The study found no detectable shift in the leading mode of atmospheric variability under
90 global warming scenarios. On the other hand, Müller and Roeckner (2008) found a strong positive
91 trend in the NAO in the ECHAM5/MPI-OM simulations. As a consequence of such uncertainties,
92 the IPCC AR5, has expressed only medium confidence in near-term projections of NAO changes
93 (IPCC, 2013).

94 Recently, atmospheric variability in the North Atlantic and the NAO pattern have also been
95 linked to Rossby wave-breaking in the upper troposphere and to atmospheric blocking (e.g., Croci-
96 Maspoli et al., 2007; Woollings et al., 2008). The term *atmospheric blocking* is broadly used to
97 describe situations in which the prevailing westerly flow is blocked, or distorted by a persistent,
98 quasi-stationary anticyclone (e.g., Rex, 1950; Berrisford et al., 2007). However, the exact
99 definition varies among studies. For example, Pelly and Hoskins (2003) pioneered the use of
100 potential vorticity (PV) as an indicator for blocking, linking blocking occurrences to the meridional
101 potential temperature gradient on a constant PV surface. In this framework, atmospheric blocking is

102 therefore associated with Rossby wave breaking. It has been shown that different blocking patterns
103 correspond to significantly different large-scale atmospheric circulations over the North Atlantic
104 basin (Rex, 1950). Blocking situations are often responsible for stagnant atmospheric conditions
105 that lead to the accumulation of pollutants at ground levels. This increases the likelihood of
106 exceeding particulate matter (PM) annual and daily limit concentrations, such as those imposed by
107 European regulations (Directive 2008/50/EC).

108 *The aim of this paper is to disentangle the role of future aerosol and GHG concentration*
109 *changes in altering atmospheric circulation, expanding earlier analysis that focussed on global*
110 *scale climate impacts (Kloster et al., 2009) and the relationship between air pollution mitigation*
111 *and extreme events (Kloster et al., 2009; Sillmann et al., 2013)*. We focus on the extreme case that
112 by 2030 aerosol concentrations will be globally reduced to the maximum feasible extent by using
113 all presently available end-of-pipe technology, using the results of an aerosol-atmosphere model
114 coupled with a mixed-layer ocean. Finally, we evaluate the impact of such atmospheric circulation
115 changes onto PM variability. *The analysis includes simulations in which only GHG*
116 *concentrations, only aerosol emissions or both are changed. In each simulation the*
117 *anthropogenic emission scenarios used to force the model are constant for the entire length of*
118 *the integration; hence, the changes in variability depicted by the model will be associated with*
119 *changes in atmospheric circulation only*. We investigate how GHG and/or aerosol forcings act on:
120 (i) the structure of the SLP meridional dipole over the North Atlantic in terms of strength and
121 location of its centres of action; (ii) changes in the NAO in the near future; (iii) the spatial structure
122 and frequency of atmospheric blocking in the North Atlantic. Finally, we also examine (iv) **how**
123 **future changes in atmospheric circulation could impact air quality over Europe.**

124 This work is structured as follows: Sect. 2 describes the models used, the simulation set-up and
125 the statistical tools adopted; Sect. 3 presents the GHG and aerosol-induced changes in the
126 magnitude and spatial pattern of the meridional SLP dipole in the North Atlantic. We also discuss
127 the related changes in the NAO and atmospheric blocking over the Atlantic, and the effects of such
128 changes on PM variability. Discussions and conclusions are presented in Sect. 4.

129 2 METHODS

130 2.1 Climate Model

131 We have analysed the climate simulations performed by Kloster et al. (2008, 2009) using the
132 ECHAM5-HAM aerosol-climate model. *We focus on the analysis of hitherto unexplored aspects*
133 *of atmospheric circulation changes over the North Atlantic. These simulations were also used by*
134 *Sillmann et al. (2013) to analyse how changes in precipitation impact on aerosol concentration;*

135 *however, they focused on annual means and did not consider to what extent these changes were*
136 *reflected by large-scale circulation changes that were driving the more localized precipitation*
137 *responses.*

138 The ECHAM5-HAM modelling system includes the atmospheric general circulation model
139 ECHAM5 (Roeckner et al., 2003) coupled to a mixed layer ocean (Roeckner et al., 1995), and the
140 microphysical aerosol model HAM (Stier et al., 2005). *The ECHAM5-HAM simulations analysed*
141 *in this study (Kloster et al., 2008, 2009) account for both the direct and indirect (cloud lifetime*
142 *and cloud albedo effect) aerosol effects.* ECHAM5 was run on a T63 horizontal grid (about 1.8° on
143 a Gaussian Grid), and on 31 vertical levels from the surface up to 10 hPa. A cloud scheme with a
144 prognostic treatment of cloud droplet and ice crystal number concentration (Lohmann et al., 2007)
145 provided fractional cloud cover prediction from relative humidity (Sundquist et al., 1989). The
146 shortwave radiation scheme included 6 bands in the visible and ultraviolet spectra (Cagnazzo et al.,
147 2007).

148 The microphysical aerosol module HAM treats the aerosol size distribution, mixing state and
149 composition as prognostic variables. It predicts the evolution of an ensemble of interacting aerosol
150 modes and is composed of the microphysical core M7 (Vignati, 2004); an emission module for SO₂,
151 black and organic carbon, and mineral dust particles; a sulphur oxidation chemistry scheme using
152 prescribed oxidant concentrations for OH, NO₂, O₃ and H₂O₂ (Feichter et al., 1996); a deposition
153 module; and a module defining the aerosol radiative properties. *Prescribing oxidant*
154 *concentrations, most importantly H₂O₂, may have led to an underestimate in the resulting sulfate*
155 *burden, since the use of off-line H₂O₂ may not accurately account for depletion by aqueous*
156 *reactions with SO₂ and recovery in cloud-free conditions. This will increase the gas-phase*
157 *production of SO₄, which is less susceptible to scavenging, and increase the SO₄ burden (Barth et*
158 *al., 2000; Roelofs et al., 1998). Another model evaluation of the effect of including explicit*
159 *oxidation (Pham, 2005) suggested an overall decline of SO₄ burden (<1 %), but an increase of*
160 *SO₄ surface concentrations (ca. 5% in many regions), due to a combination of increased near-*
161 *surface oxidation and removal processes. This is a relatively minor error compared to other*
162 *uncertainties (Textor et al., 2007). The aerosol optical properties were explicitly simulated using*
163 *Mie theory and provided as input for the radiation scheme in ECHAM5 following Toon and*
164 *Ackerman (1981). Climate-sensitive natural emissions (dimethyl sulphide, sea salt and dust) were*
165 *simulated interactively.*

166 **2.2 Simulation Set-up**

167 The GHG concentrations used in the simulations were derived from the IMAGE 2.2
168 implementation of the SRES B2 scenario (IMAGE-team, 2001). The SRES B2 storyline describes a
169 world with intermediate population and economic growth, in which the emphasis is on local
170 solutions to economic, social, and environmental sustainability.

171 The anthropogenic emissions of carbonaceous aerosols, namely black carbon (BC) and organic
172 carbon (OC), as well as sulphur dioxide (SO_2), the main precursor of sulphate aerosols, are
173 extracted from an aerosol emission inventory developed by the International Institute for Applied
174 System Analysis (IIASA). In this work, a Maximum Feasible Reduction (MFR) air pollutant
175 emission scenario was explored for the year 2030 (Cofala et al., 2007). MFR assumes the full
176 implementation of the most advanced available technologies for aerosol emissions abatement. It is
177 built using projections of human activity levels (industrial production, fuel consumption, livestock
178 numbers, crop farming, waste treatment and disposal) based on current national perspectives on the
179 economic and energy development up to the year 2030. In regions where data were not available,
180 the economic and energy future trends estimated in the IPCC SRES B2 MESSAGE scenario
181 (Nakicenovic et al., 2000; Riahi and Roehrl, 2000) were considered. Biomass burning emissions,
182 both anthropogenic and natural, were assumed to stay constant at 2000 levels. Changes in land use
183 were not taken into account.

184 In the present study the modifications of future North Atlantic atmospheric circulation are
185 assessed by analysing the differences between near future (year 2030) and present-day (year 2000)
186 conditions reproduced in climate equilibrium simulations. A 60-yr control simulation was
187 performed with GHG concentrations, aerosol and aerosol precursor emissions of the year 2000, and
188 three 30-yr sensitivity ***equilibrium experiments*** were performed, using three different combinations
189 of GHG concentrations and aerosol emissions scenarios:

- 190 • 2000 experiment: year 2000 GHG concentrations and aerosol emissions;
- 191 • 2030 experiment: year 2030 GHG concentrations and MFR aerosol emission scenario;
- 192 • 2030GHG experiment: year 2030 GHG concentrations, and 2000 aerosol emissions;
- 193 • 2030AER experiment: year 2000 GHG concentrations, and 2030 MFR aerosol emission
194 scenario.

195 All simulation used a spin-up of 30 years, not included in the analysis.

196 ***The 2030GHG and 2030AER experiments in which, respectively, aerosol emissions and***
197 ***GHG concentrations remained at the 2000 level, were performed to separate the effects of GHG***
198 ***concentrations and aerosols emissions.*** The experimental setups are summarized in Table 1.

199 **2.3 Statistical analysis methods**

200 We evaluate three aspects of the large-scale circulation: 1) the SLP spatial structure (shift of
201 centres of action); 2) the leading mode of atmospheric variability (NAO); and 3) the blocking
202 frequency. Finally, we investigate how the atmospheric circulation changes affect PM distributions.

203 To investigate the impact of aerosol and GHG concentration changes on SLP spatial structure,
204 we define the SLP centres of action for the winter season (January, February and December, DJF)
205 by creating SLP coherence maps (Pausata et al. 2009). The coherence index value ($0 \leq CI \leq 1$) at each
206 grid-point is the absolute value of the area-averaged correlation between the monthly SLP time-
207 series at that point and over the rest of the North Atlantic basin (20°N - 85°N ; 90°W - 40°E). Higher
208 values indicate that the SLP variability at that location is more *coherent* with variability throughout
209 the North Atlantic, either in-phase or anti-phase. ***The Northern and Southern SLP Centres Of***
210 ***Action (NCOA and SCoA) are identified as CI maxima over the North (north of 55°N) and***
211 ***subtropical Atlantic (south of 55°N), respectively.*** This method allows determining the spatial
212 distribution and shifts of the COAs due to aerosol and GHG concentration changes, both in
213 combination and separately (for details see Appendix A). In order to verify that the computed
214 geographical shifts in the centres of action are outside the normal range of inter-annual variability,
215 we use a statistical bootstrap approach to produce a set of 100 CI maps for the 2000 experiment. ***We***
216 ***randomly select subsamples of 20 years for the 30-year long simulations and subsamples of 40***
217 ***years for the 2000 (60-year long) simulation, and perform the CI analysis for each subsample.***
218 ***Subsequently, we apply the Student's t-test to determine whether the CI pattern and the shift in***
219 ***the centres of actions between the 2000 control simulation and the sensitivity studies are***
220 ***significant at 95% confidence level.***

221 ***Furthermore, in order to assess the variability of the SCoA and evaluate its relation to***
222 ***blocking frequency and precipitation in the 2000 simulations, we construct an index of the SCoA***
223 ***(SCOAI). We first generate 10000 random subsamples of 15 years from the 60-year pool of the***
224 ***2000 simulation. In this case we have reduced the subsample size from 40 to 15 years in order to***
225 ***increase the variability of the SCoA and hence, better understand its influence on blocking***
226 ***frequency and precipitation. We then calculate the CI values and determine the position of the***
227 ***SCoA (maximum in the CI south of 55°N) for each subsample. Hence, we construct the SCOAI***
228 ***where the value of 0 is defined as the 50th percentile of the SCoA position within the 10000***
229 ***subsamples. Eastward positions (relative to the 50th percentile) of the SCoA are defined as***
230 ***positive values of the SCOAI and westward position as negative ones. The SCOAI has then been***
231 ***normalized by the standard deviations of the eastward and westward SCoA positions.***

232 Winter changes in the leading mode of atmospheric variability are investigated by using the
233 monthly NAO Index (NAOI), defined as the difference in the normalized SLP anomalies between
234 Ponte Delgada, Azores, and Stykkisholmur/Reykjavik, Iceland. The NAOI allows to look for shifts
235 in the North Atlantic atmospheric circulation associated with future climate change (Hurrell, 1995).

236 The analysis of blocking frequency over the North Atlantic basin is performed as follows. In
237 order to define atmospheric blocking, the present paper utilizes a bi-dimensional index that
238 identifies reversals in the meridional gradient of 500 hPa geopotential height (Davini and Cagnazzo,
239 2013; Davini et al., 2012; Tibaldi and Molteni, 1990). For every model gridbox with coordinates
240 (*latitude* = φ , *longitude* = λ), the following two quantities are defined:

$$241 \quad \Delta_N(\varphi, \lambda) = \frac{Z_{500}(\varphi, \lambda) - Z_{500}(\varphi - 15^\circ, \lambda)}{15^\circ},$$

$$242 \quad \Delta_S(\varphi, \lambda) = \frac{Z_{500}(\varphi + 15^\circ, \lambda) - Z_{500}(\varphi, \lambda)}{15^\circ},$$

243 over the domain where $30^\circ N < \varphi < 72.5^\circ N$, $180^\circ W < \lambda \leq 180^\circ E$. **In order for a gridbox to be**
244 **flagged as ‘blocked’, the following must hold:**

$$\Delta_N > 0; \Delta_S < -10 \text{ m/}^\circ \text{ latitude}$$

245 *In order to define a blocking event, a number of additional constraints are also enforced.*
246 *Firstly, a cluster of adjacent blocked gridboxes spanning at least 15° longitude must be identified*
247 *at a given timestep. Therefore, if a gridbox is blocked in isolation, it is not considered to be part*
248 *of a blocking event. A persistence criterion is also applied: a blocking event requires that at least*
249 *another blocked gridbox is detected for 5 consecutive days within an area of 5° latitude by 10°*
250 *longitude, centred on the original blocked gridbox.*

251 *The impacts of changes in atmospheric circulation on air pollution are investigated by*
252 *analysing changes in PM monthly anomaly distributions. We focus on changes in the skewness*
253 *of distributions for the winter season. The skewness is the distribution’s third standardized*
254 *moment, and is a measure of the asymmetry of the distribution. Positive skewness values typically*
255 *indicate that the right side tail of the distribution becomes longer than the left side, and vice-*
256 *versa for negative values. Significance in the skewness differences is assessed by using a*
257 *Kolmogorov-Smirnov test at 95% confidence level. This test is a non-parametric tool, meaning*
258 *that it makes no assumptions on the shape of the data distribution. An ‘artificial’ variability is*
259 *introduced in the skewness values in each simulation through a bootstrap technique. For each*
260 *experiment, we calculate the skewness values of 100 random distributions, generated from the*
261 *original pool of 30 or 60 years using the same bootstrap technique described for the CI. The*
262 *significance level is then identified based on this sample.*

263 **3 RESULTS**

264 The results presented here describe the effects of GHG and aerosol concentrations on the mean
265 state and variability of the North Atlantic atmospheric circulation. The results are presented in three
266 sections. In the first section, changes in the spatial structure of the SLP and its variability are
267 investigated. In the second section, we extend the analysis to changes in the blocking frequency.
268 Finally, in the third section, we quantify the impacts of such changes on precipitation regime and
269 PM variability.

270 **3.1 Changes in SLP centres of action and their variability**

271 The 2030 and 2030AER simulations show a north-eastward shift of the SCOAs compared to the
272 2000 control simulation (Fig. 1). The area of highest SLP coherence in the 2000 simulation is
273 located in the central-western part of the sub-tropical North Atlantic, whereas in the 2030
274 simulation it is shifted off the coast of northern Morocco. The NCOA, instead, remains located in
275 central western Greenland for all scenarios. However, in the 2030 and 2030AER simulations, a
276 secondary CI maximum develops in the Norwegian Sea, and the areas with the CI maxima are
277 broader. Secondary CI maxima also develop at low latitudes compared to the 2000 simulation (Fig.
278 1).

279 Both sensitivity simulations (2030GHG and 2030AER) show a significant north-eastward shift
280 (see section 2.3) of the SCOAs as well as broader areas of CI maxima compared to the 2000
281 simulation. Both these features are more pronounced in the 2030AER than in the 2030GHG
282 simulation, in particular the displacement towards the Mediterranean Sea of the SCOAs.

283 *With regard to the SLP variability, the 2030 simulation shows a significant positive shift of
284 the NAO mean state by 0.46 compared to the 2000 control period (Fig. 2). The probability of
285 having an NAOI greater than +1 increases from 30% to 40% (Fig. 2). Neither the GHG increase
286 (2030GHG) nor the aerosol reduction (2030AER) have any statistically significant role in
287 changing the NAO mean state and the frequency distribution of strongly positive/negative NAO
288 phases relative to the control simulation. Nevertheless, the GHG increase seems to provide a
289 stronger contribution to the NAO shift; the 2030AER NAO shift is significant at 65% confidence
290 level, while the 2030GHG one at 85% confidence (using a t-test). Only the combination of both
291 2030 GHGs and aerosol emissions leads to a statistically significant change in the NAO mean
292 state at 95% confidence level.*

293 *Hence, whereas the NAO shift is related to both aerosol and GHG changes (with likely
294 stronger impacts from the GHGs), the aerosol reduction alone plays the largest role in shifting
295 the southern centre of action of SLP towards the Mediterranean.*

296 **3.2 Changes in blocking frequency**

297 Blocking events can have a large impact on weather patterns and sometimes lead to the
298 occurrence of extreme events (e.g., Yiou and Nogaj, 2004); hence, it is important to quantify the
299 variability and possible changes in the preferred location of blocking occurrences.

300 The 2000 simulation shows a blocking frequency that peaks in the south over the sub-tropical
301 North Atlantic (low-latitude blocking, LLB) and in the north over Greenland (high-latitude
302 blocking, HLB), as shown in Figure 3a. The LLB events are linked to a northward displacement of
303 the subtropical high-pressure system. The HLB events are characterized by long durations (on the
304 order of 9 days), diverting the main flow southward (Davini et al., 2012). The simulated 2000
305 blocking climatology is slightly different from the patterns seen in re-analysis data, which have a
306 higher activity over the Nordic seas, but nevertheless shows a strong resemblance to the observed
307 climatology (cf. Fig. 3a with Fig. 1 in Davini et al., 2012a).

308 *HLBs and LLBs are strongly tied to the phase of the NAO: Woollings et al. (2008) showed
309 that HLB events over Greenland are strongly anti-correlated with the NAOI. Furthermore,
310 changes in the HLB position (Wang and Magnusdottir, 2012) and frequency (Davini et al.,
311 2012b) have been shown to influence not only the NAOI, but also its pattern. Yao and Luo
312 (2014) have described the relationship between HLBs and LLBs and the NAO phase in winter
313 during the period 1950-2011. The HLBs are connected not only to the NAO phase but also to the
314 position of the SCoA. By regressing the NAOI and the SCoAI time-series onto the blocking
315 frequency field in the 2000 simulation (see details in Appendix B), we analyze how the NAO
316 phase and the position of the SCoA affect the blocking frequency. Positive NAO phases are
317 associated to a northward increase of LLBs (Fig. 4a), whereas eastward positions of the SCoA
318 are connected to a northeastward increase of LLBs (Fig. 4b). The regression analysis also shows
319 a decreased HLB frequency over Greenland during positive NAO phases in agreement with the
320 above-mentioned studies.*

321 *The 2030 simulation shows a significant increase (up to 50-70%) in the number of LLB
322 events over western Europe and the Mediterranean basin, corresponding to a more invasive
323 subtropical anticyclone (high-pressure system) over southern and central Europe in winter. The
324 increased LLB frequency in the 2030 simulation is consistent with both a positive NAO shift
325 (Fig. 4a) and an eastward shift of the SCoA (Fig. 4b). On the other hand, HLBs decrease (Fig.
326 3b) is in agreement with the reduction in negative NAO phases discussed in Section 3.1 and the
327 NAOI-blocking frequency relationship highlighted in figure 4a.*

328 *The 2030GHG and 2030AER simulations also show significant increases in the LLB
329 frequency over the mid-latitude North Atlantic and decreases in the HLB frequency (Fig. 3c and*

330 *3d). However, the patterns are different from one another: the high-latitude change in both*
331 *2030GHG and 2030 closely approximates the blocking frequency difference between the positive*
332 *and negative phases of the NAO, shown in figure 4a (cf. with figure 3b and 3c). On the other*
333 *hand, the HLB frequency change in the 2030AER experiment seems to be related to a shift in the*
334 *SCOA (cf. 3d and 4b). This is consistent with the large (small) eastward displacement of the*
335 *SCOA in the 2030AER (2030GHG) simulation and the smaller (larger) shift in the NAO mean*
336 *state.*

337 *The 2030AER simulation also shows a significant increase in LLB frequency over the*
338 *Mediterranean, not seen in the 2030GHG experiment. Hence, the aerosol concentration*
339 *reduction seems to be the main driver of the increase in LLB events over the Mediterranean seen*
340 *in the 2030 simulation (Fig. 3 cf. panels b and d).* These results strengthen the role of aerosols in
341 affecting atmospheric dynamics in the North Atlantic, suggesting that they drive both a) an
342 eastward shift of the southern centre of action of SLP and b) an increased tendency of the sub-
343 tropical anticyclone to expand towards the Mediterranean Sea.

344 3.3 Impacts on air-quality

345 *Large-scale changes in atmospheric circulation can affect PM variability over Europe by*
346 *altering the precipitation regime. The latter is one of the main mechanisms for PM removal, and*
347 *affects PM concentrations at the surface (e.g., Horton et al., 2014; Jacob and Winner, 2009;*
348 *Pausata et al., 2013).* For example, an eastward shift of the SCOA and/or a shift towards positive
349 NAOI, together with an increased frequency of blocking events in the Mediterranean, may lead to a
350 higher frequency of dry, stagnant weather conditions in south-western Europe, thus worsening air
351 quality (see Appendix C for a discussion on the relationship between circulation changes and
352 precipitation). Hence, even though there will be an overall improvement in air quality conditions
353 associated with an abatement of PM emissions, additional PM emission reduction measures may be
354 necessary for those countries and cities lying in the Mediterranean area to counterbalance the effects
355 of the atmospheric circulation changes. This hypothesis has already been suggested by Pausata et al.
356 (2013) on the basis of an NAO-PM analysis using the same model driven by ERA-40 re-analysis
357 data. *In this work, we test it further by analyzing climate sensitivity experiments under different*
358 *aerosol emission scenarios for the near future. We aim to provide a general coherent overview of*
359 *the impacts of large-scale circulation changes on air-quality. We focus on monthly PM data,*
360 *similar to the monthly SLP field used for the NAOI and CI analyses. We do not discuss the daily*
361 *exceedances of EU thresholds, since this would be beyond the scope of the present study, and the*
362 *coarse resolution global model has limited skills on simulating them (Pausata et al., 2013).*

363 *To quantify how the changes in atmospheric circulation affect air-quality, we calculate the*
364 *relative anomaly distributions of PM concentrations for four regions (see also figure 3a), to*
365 *encompass the different areas of influence of the NAO over Europe:*

- 366 • Western Mediterranean (WM): 34°N-43°N / 0°-10°W;
- 367 • Eastern Mediterranean (EM): 34°N-43°N / 10°E-40°E;
- 368 • Central Europe (CE): 44°N-53°N / 0°-15°E;
- 369 • Eastern Europe (EE): 46°N-60°N / 20°E-40°E.

370 In the PM we have considered only the aerosol components included in ECHAM5-HAM that
371 have a predominantly anthropogenic signature – namely black and organic carbon, and sulphates –
372 disregarding aerosols of natural origin (e.g., sea-salt, mineral dust). Thus, the PM in this paper
373 represents mostly PM_{2.5}, and is likely a lower bound on the ‘real’ PM concentrations (for an
374 evaluation of correspondence between modelled and measured PM_{2.5}/PM₁₀ see the Supplementary
375 Material in Pausata et al., 2013).

376 First, we analyse the skewnesses of the monthly PM relative anomaly distributions for the
377 winter season. PM relative anomaly distributions for all experiments and for all four regions show
378 positive skewness values, meaning that positive PM anomalies are becoming more likely than
379 negative ones (Fig. 5 and Table 2). Our results show that, in all three 2030 experiments, the
380 simulated PM distributions change significantly in all regions considered due to the altered
381 atmospheric circulation (Fig. 5 and Table 2).

382 *In the Western Mediterranean (WM), the PM relative anomaly skewness increases*
383 *remarkably from 0.26 in the 2000 case to 1.02 and 1.05 in the 2030 and 2030AER simulations,*
384 *respectively. This change is mainly led by the aerosol reduction, whereas the GHGs only drive a*
385 *small contribution (Table 2). The large change in skewness in the 2030 simulation is*
386 *accompanied by a corresponding shift in the upper and lower percentiles of the distribution. The*
387 *5th and 95th percentiles rise by 8% and 4% respectively relative to 2000, indicating a transition*
388 *towards more positive PM anomalies (Table 3). The rise in PM extremes matches the changes in*
389 *rainy day extreme percentiles (not shown). The 95th and 5th percentiles of the frequency of rainy*
390 *days decrease by 2% and 17% respectively. Rainy day frequencies and PM anomalies are anti-*
391 *correlated; therefore, a change in the 95th (5th) percentile in rainy days should be associated with*
392 *a change of the opposite sign in the 5th (95th) percentile in the PM anomalies.*

393 *The Eastern Mediterranean (EM) also experiences an increased skewness in the 2030*
394 *simulation relative to 2000. However, the changes are smaller compared to the WM, possibly*
395 *because of the greater distance from the SCoA – located off the coast of the Iberian Peninsula in*

396 *the 2030 simulation – and the contrasting effect of the NAO phase inside the domain: as one
397 moves further to the east in the Mediterranean basin, the correlation between NAO and
398 precipitation changes sign (Fig. B1a). The smaller changes in the PM distribution simulated in
399 the EM compared to the WM could therefore be related to a different behaviour in precipitation
400 regime (see Appendix B).*

401 *On the other hand, Central (CE) and Eastern Europe (EE) show a decreased skewness in the
402 2030 case compared to the 2000 simulation. CE displays a shift in skewness from 1.44 to 0.66;
403 the corresponding shift in EE is from 1.70 to 1.18. Furthermore, CE also shows an increment in
404 the number of negative extremes, with a 14% decrease in the 5th percentile. However, CE also
405 experiences an increase in positive extremes with a +7% shift in the 95th percentile in the 2030
406 simulation compared to the 2000 experiment (Table 3). The change in the extreme PM
407 percentiles is accompanied by a similar but opposite change in the rainy day percentiles: +3%
408 and -9% for the 95th and 5th percentiles, respectively. CE is located closer to the transition area of
409 the NAO influence between northern Europe and Mediterranean basin (see also figure B1).
410 Therefore, this area may be exposed to alternation of a more invasive Azores high and rainy
411 Atlantic storms.*

412 Therefore, the regions that will be most affected by future large-scale circulation changes are
413 the Western Mediterranean and Central Europe, both with increased high PM concentration
414 episodes, but the latter also with a strong increment in low PM values relative to 2000. The
415 implications of these results for air quality policy are discussed in the following section.

417 4 Discussions and Conclusions

418 The present study analyses future scenarios of atmospheric circulation over the North Atlantic
419 and possible impacts on air quality over Europe. The chemistry-atmosphere ECHAM5-HAM
420 model, coupled to a mixed layer ocean, shows a change towards more positive NAO phases,
421 together with an eastward shift of the southern SLP centre of action. ***These shifts are associated to
422 an increased frequency of blocking events over the western Mediterranean.*** Our results highlight
423 how the decreased aerosol and aerosol precursor emissions, along with GHGs, are responsible for
424 changes in radiative forcing that feedback onto the atmospheric circulation and alter the NAO mean
425 state. ***Table 4 provides a qualitative summary of the atmospheric changes induced by 2030
426 GHGs, aerosols and jointly by GHG and aerosol emissions on a variety of circulation indicators.***
427 These changes in atmospheric circulation in turn feedback significantly on air quality, leading to an
428 increase in extreme pollution events over the western Mediterranean.

429 Future shifts in the NAO phase have already been discussed by several modelling studies (e.g.,
430 Gillett and Fyfe, 2013; Karpechko, 2010; Stephenson et al., 2006; Kuzmina, 2005; Hu and Wu,
431 2004); however, the driving mechanisms behind these shifts are still debated. Hori et al. (2007)
432 have shown that NAO variability does not change substantially in the SRES-A1B scenarios
433 compared to the 20th century, and conclude that the trend in the NAO index is the result of an
434 anthropogenic trend in the basic mean state, rather than being due to changes in NAO variability.
435 Our results support Hori et al.'s (2007) findings by showing that anthropogenic changes in GHG
436 and aerosols lead to a change in the NAO's mean state rather than its variability (Fig. 2).

437 The positive NAO shift comes along with a shift of the SLP centres of action. Hilmer and Jung
438 (2000) have found an eastward shift in the SLP pattern associated with the inter-annual variability
439 of the NAO from 1958-1977 to 1978-1997. Peterson et al. (2003) have suggested that this shift is
440 simply a consequence of the trend towards a more positive NAO index in the last two decades of
441 the 20th century. Hu and Wu (2004), using both data and a coupled general circulation model, have
442 also shown that a shift of both SLP centres of action took place in the second half of the last
443 century, which will likely continue in the future. Our study confirms that this shift also occurs under
444 a global warming scenario. However, while in our simulations the southern centre undergoes a
445 remarkable eastward shift, the northern one is fairly stable around southern Greenland – as
446 demonstrated using the coherence index approach (Fig. 1). Nevertheless, the CI maps do show that
447 in the 2030 simulations a secondary northern maximum – not present in the 2000 experiment –
448 appears in the Norwegian Sea (Fig. 1). ***Furthermore, our simulations highlight how the future
449 abatement of the aerosol load may play an important role in the eastward shift of the SLP centres
450 of action.***

451 The present study also finds an increased blocking frequency over the western Mediterranean.
452 Such increase, together with an eastward displacement of the southern SLP centre of action and a
453 positive shift of the NAO mean state, leads to more frequent stagnant weather conditions that favour
454 pollutant accumulation in the Mediterranean. This change in frequency of pollution events has also
455 been described by Kloster et al. (2009), who showed that aerosol abundance is dependent on the
456 climate state, as also highlighted in a number of other modelling studies (e.g., Feichter et al., 2004;
457 and overview in IPCC, 2013). Kloster et al. (2009) further found that aerosol burdens increase in
458 the area due to less precipitation and reduced wet-deposition. Hence, they suggest that climate
459 change alone would worsen air pollution by aerosols. Here we show that in Europe these findings
460 are consistent with a straightforward NAO-behaviour analysis, and that indeed a positive shift in
461 future NAO may lead to more positive extreme pollution events over specific areas, such as in the
462 western Mediterranean countries. This result also supports the hypothesis of Pausata et al. (2013)

463 that climate change will lead to more extreme pollution events over the western Mediterranean,
464 forcing southern European countries to implement more stringent abatement measures to counteract
465 adverse changes in PM variability. However, our study also highlights that the increase in the
466 number of high PM episodes in the western Mediterranean is partially counterbalanced by a lower
467 median and a narrowing of the PM frequency distribution around the median itself (Fig. 5 and Table
468 3).

469 Current European legislation considers PM air quality thresholds of $25 \mu\text{g}/\text{m}^3$ (annual average)
470 for $\text{PM}_{2.5}$, and $50 \mu\text{g}/\text{m}^3$ for PM_{10} (24 hours, not to be exceeded for more than 35 days per year).
471 European legislation has also set an indicative target value for $\text{PM}_{2.5}$ annual average of $20 \mu\text{g}/\text{m}^3$.
472 Currently, between 20-31% and 22-33% of the urban population in Europe is exposed to $\text{PM}_{2.5}$
473 levels above the $20 \mu\text{g}/\text{m}^3$ threshold (EEA, 2013). However, more stringent standards are currently
474 in place in the USA (annual $\text{PM}_{2.5}$: $12 \mu\text{g}/\text{m}^3$), or recommended by the World Health Organization –
475 WHO (annual $\text{PM}_{2.5}/\text{PM}_{10}$: $10/20 \mu\text{g}/\text{m}^3$), and may be adopted in Europe as well at some point in
476 the future. Considering the more stringent WHO guidelines, currently between 91-96% ($\text{PM}_{2.5}$) and
477 85-88% (PM_{10}) of urban population is exposed to values above the thresholds
478 (<http://ec.europa.eu/environment/air/quality/standards.htm>). Depending on threshold levels set by
479 future EU air quality legislation, it is not *a-priori* clear how changes in PM frequency distributions
480 will affect exceedance of these thresholds, and what levels of emission reductions are appropriate to
481 reach these air quality objectives.

482 Unfortunately, our coarse resolution global model results only allow a qualitative assessment of
483 the impact on air quality exceedance of future air pollution emissions and climate change.
484 Therefore, we envision the need for more in-depth studies to further quantify the significance of our
485 findings with respect to the relationship between future changes in atmospheric circulation and air-
486 quality related issues. These studies should make use of both high vertically resolved coupled
487 atmosphere-ocean general circulation models and regional air-quality models. The former models
488 are needed to better quantify anthropogenic-induced changes in atmospheric circulation and their
489 impacts on air quality, given the strong coupling between stratospheric and tropospheric circulation
490 (e.g., Hoerling et al., 2001; Scaife et al., 2005; Omrani et al., 2013). The latter models can better
491 constrain the effects of the altered atmospheric circulation on air-quality at regional scales. The
492 aerosol 2030 simulations used in this study assumed the MFR scenario; the extent to which these
493 maximum-feasible air pollutant emission reductions will actually happen depends on the
494 effectiveness of policies. Nevertheless, 60-70% of the reduction (compared to a 2000 baseline)
495 assumed by the MFR scenario is not unrealistic and hence some of the feedbacks seen in this study
496 are likely to be witnessed in the real world. Most of the EU estimates of benefits related to pollution

497 reduction (e.g., a decrease in the number of premature deaths) are determined without taking into
498 account the potential effect of a future atmospheric circulation changes. Therefore, more
499 quantitative studies in which high-resolution regional air quality models are coupled to global
500 ocean-atmosphere-chemistry climate models are necessary to assess the climate feedbacks on
501 aerosol abatement. Understanding and characterizing changes in the NAO in global models, thus,
502 providing meteorological and chemical boundary conditions for regional air quality models, will
503 also allow for a better analysis of exceedance rates of air quality standards associated with the inter-
504 annual variability of circulation patterns.

505 ***Appendix A***

506 *In Appendix A we explain in detail the relationship between the coherence index (CI)
507 analysis and the NAO. The CI analysis of the SLP field identifies the areas that best correlate
508 with the SLP variability over a given basin. In other words, the maxima in the CI represent the
509 points that best capture SLP variability within a given domain. On the other hand, the NAOI is a
510 measure of the wintertime SLP swings between two specific points in the North Atlantic, located
511 in the "eye" of the two stable pressure areas, the Azores high and Icelandic low. Therefore, these
512 two locations capture a substantial amount of SLP variability in the basin. Pausata et al. (2009)
513 have already shown how the CI and the NAOI are connected to each other in the present climate.
514 The CI patterns of surface temperature (precipitation) closely resemble the correlation patterns
515 between surface temperature (precipitation) and the leading Principal Component (PC1) of the
516 SLP field (which is an alternative definition of the NAOI; see figures 7 and 8 in Pausata et al.,
517 2009). To further demonstrate the link between the CI and NAOI, we have calculated the
518 correlation between SLP and the leading PC of the SLP field, following Pausata et al. (2009).
519 For simplicity, in the manuscript we have used the canonical definition of the NAOI, since the
520 PC1 and NAOI in winter are highly correlated ($r > 0.90$, see also Hurrell, 1995). Figure A1
521 shows that the correlation between the PC1 and SLP is very similar to the CI pattern and the
522 correlation maxima of both analyses are quite close to each other (cf. Figs A1 and 1a). The
523 advantage of the CI analysis compared to the PC/SLP (or temperature or precipitation)
524 correlation analysis is that the CI analysis does not depend only on the leading mode of
525 variability but directly integrates all other modes that directly affect the fluctuations of the
526 analyzed variable.*

527 *Pausata et al. (2009) have also shown that, during different climate states in which the
528 leading mode of SLP variability (PC1) is less dominant (lower explained variability of the EOF1),
529 the CI and the PC correlation patterns can be completely different. Therefore, we have decided to
530 adopt the CI in addition to the canonical NAOI as a further metric to better understand and*

531 interpret large-scale circulation changes.

532

533 **Appendix B**

534 *In Appendix B, we examine how the large-scale atmospheric indicators used in this study are*
535 *related to the number of rainy days in DJF over Europe. PM concentrations at the surface can*
536 *be affected by different factors such as precipitation or the thermal structure of the boundary*
537 *layer. However, these factors are implicitly included in the large-scale changes in atmospheric*
538 *circulation, i.e. the changes in the CI pattern, NAO phase and blocking events. In order to study*
539 *the degree to which rainy day anomalies are associated to the NAO phase and the position of the*
540 *southern SLP centre of action (SCOA) in the 2000 simulation, we use a regression analysis: a*
541 *regression coefficient $b(i,j)$ is calculated at each specific latitude (i) and longitude (j) by linearly*
542 *regressing the input variable of interest (rainy days(t,i,j) anomalies) against the reference time*
543 *series (NAOI(t) or SCOA Index – SCOAI(t)).*

544 *The corresponding regression map is a composite field consisting of a linear combination of*
545 *all available data, where each datum (e.g. rainy day anomaly) is weighted by the concurrent*
546 *value of the INDEX (NAOI or SCOAI) time series:*

547

$$b(i,j) = \left(\frac{1}{N}\right) \times \sum_{t=1}^N [Rday^{anom}(t, i, j) \times INDEX(t)],$$

548

549 *where N is the number of time samples. The $b(i,j)$ coefficients may be viewed as the*
550 *perturbations in rainy day frequency at the $(i,j)^{th}$ grid point observed in association with a positive*
551 *perturbation in the INDEX(t) (NAOI(t) or SCOAI(t) by one standard deviation (i.e.*
552 *NAOI/SCOAI = 1) (Lim and Wallace, 1991). For simplicity, we only show the anomalies*
553 *associated with positive NAO (SCOA) phases; by construction, the anomaly pattern associated*
554 *with the negative NAO phase differs only in sign. The regressions of the NAOI and SCOAI*
555 *clearly show the influence of both the NAO phase and the position of the SCOA on rainy day*
556 *frequency (Fig. B1). Positive NAO phases and SCOAs shifted to the east lead to decreased*
557 *numbers of rainy days over the central-western Mediterranean and increases over part of central*
558 *Europe. The opposite influence is found for the eastern Mediterranean, where a positive NAO*
559 *phase is associated to an increased number of rainy days, while an eastward location of the*
560 *southern SLP maximum is linked to a decreased number of rainy days.*

561 *Finally, we related rainy day anomalies in each of the four selected regions in Europe (WM, EM,*

562 *CE and EE) to the frequency of blocking events in the Atlantic sector (30°–72°N, 80°W–45°E).*
563 *To do so, we have constructed a composite map for each domain. We take each gridpoint (X_{fd} ,*
564 *Y_{fd}) *within the full domain (entire Atlantic sector), and compute the frequency in rainy days at*
565 *each gridpoint (x_{rd} , y_{rd}) within the regional domain (WM, EM, CE or EE) while gridpoint (X_{fd} ,*
566 *Y_{fd}) *is blocked. Such values are assigned to gridpoint (X_{fd}, Y_{fd}). This calculation is then repeated**
567 *for days on which gridpoint (X_{fd} , Y_{fd}) is unblocked. An anomaly in frequency of rainy days*
568 *between the blocked and unblocked cases is then found. This means that, for each gridpoint (X_{fd} ,*
569 *Y_{fd}) *in the full domain, we have several percentage anomalies, one for each gridpoint (x_{rd} , y_{rd})**
570 *within the regional domain. To obtain the composite map for each regional domain, we then*
571 *average these values to obtain a single percentage value for each gridpoint (X_{fd} , Y_{fd}). For example,*
572 *for WM the positive values over southern Norway indicate that, when there is a blocking event*
573 *over this area, an increase in rainy days by about 10% is expected over the WM compared to the*
574 *case with no blocking over southern Norway. The value of 10% is an average over the response*
575 *at each of the gridpoints (x_{rd} , y_{rd}) within the WM domain. On the other hand, blocking events to*
576 *the west of and over the WM lead to a 10–15% increase in rainy days relative to the case with no*
577 *blocking events over the same regions (Fig. B2a).**

578 *Hence, our analysis shows, as expected, that increased numbers of blocking events over western*
579 *Europe and the eastern North Atlantic are associated with reduced numbers of rainy days over*
580 *the Iberian Peninsula, while high-latitude blockings are associated with more precipitation days*
581 *over the WM (Fig. B2a). For the EM, on the opposite, the blocking frequency over western*
582 *Europe and the eastern North Atlantic does not have a remarkable influence (Fig. B2c). This,*
583 *together with a contrasting influence on this region of the NAO and SCAO shifts (Fig. B1) may*
584 *be responsible for the sometimes apparently ambiguous change in PM anomalies simulated in*
585 *the three 2030 experiments.*

586 *This analysis shows how rainy days are connected to the large-scale circulation patterns*
587 *investigated in this study, providing a context for their impact on PM concentrations at the*
588 *surface.*

589 Appendix C

590 *In Appendix C, we examine how the number of rainy days in DJF changes in the 2030*
591 *simulations compared to the 2000 control experiment over Europe. This step will provide a better*
592 *understanding on how the atmospheric circulation changes may impact – through changes in the*
593 *number of rainy-days – PM distributions in the future. We focus on the average number of rainy*
594 *days per month during winter, because the monthly aerosol concentrations are more strongly*

595 affected by the number of rainy days (even with small precipitation amounts) rather than by the
596 total intensity of the monthly precipitation (Claassen and Halm, 1995). We define a rainy day as
597 a day with precipitation > 1 mm at a given grid-box.

598 The 2030 simulation shows a clear dipole pattern, with an increased number of rainy days
599 (up to 60%) in central-northern Europe and a reduction (up to 50%) in southern Europe, relative
600 to 2000 simulation (Fig. C1). In general, similar patterns are found in the 2030GHG and
601 2030AER cases. However, there are some remarkable differences over the British Isles, central
602 Europe and southern Norway, as well as the Mediterranean basin. The increase in rainy days in
603 the 2030AER seems to be shifted further south compared to 2030GHG, leading to more rainy
604 days over the British Isles and central Europe (2030AER) instead of the northern North Atlantic
605 and Southern Norway (2030GHG). The 2030AER simulation further shows a significant
606 decrease in rainy days confined to the central-western part of the Mediterranean and to the
607 southern North Atlantic, whereas in the 2030GHG the decrease is spread out over the entire
608 Mediterranean. The combination of the 2030GHG and 2030AER changes in rainy days
609 resembles the 2030 anomaly pattern (Fig. C1). The difference between the 2030GHG and
610 2030AER anomalies is likely related to the different changes in atmospheric circulations
611 discussed in Sections 3.1 and 3.2. The 2030GHG case experiences a more pronounced shift in
612 the NAO phase compared to the 2030AER simulation and no changes in the SCoA. The
613 2030AER, on the other hand, is characterized by a significant eastward shift of the SCoA but
614 only a small shift in the NAO (see appendix B).

615 Acknowledgements

616 FSR Pausata and FJ Dentener were funded by the EU FP7 project PEGASOS. The authors would like to
617 thank P. Davini for discussions and suggestions on the atmospheric blocking analysis.

618 References

- 619 Albrecht, B. A.: Aerosols, cloud microphysics, and fractional cloudiness., Science, 245(4923),
620 1227–30, doi:10.1126/science.245.4923.1227, 1989.
621 Barnes, E. A. and Fiore, A. M.: Surface ozone variability and the jet position: Implications for
622 projecting future air quality, Geophys. Res. Lett., 40(11), 2839–2844, doi:10.1002/grl.50411, 2013.
623 Barth, M. C., Rasch, P. J., Kiehl, J. T., Benkovitz, C. M. and Schwartz, S. E.: Sulfur chemistry
624 in the National Center for Atmospheric Research Community Climate Model: Description,
625 evaluation, features, and sensitivity to aqueous chemistry, J. Geophys. Res., 105(D1), 1387,
626 doi:10.1029/1999JD900773, 2000.
627 Berrisford, P., Hoskins, B. J. and Tyrlis, E.: Blocking and Rossby Wave Breaking on the
628 Dynamical Tropopause in the Southern Hemisphere, J. Atmos. Sci., 64(8), 2881–2898,
629 doi:10.1175/JAS3984.1, 2007.

- 630 Cagnazzo, C., Manzini, E., Giorgetta, M. A., Forster, P. M. D. F. and Morcrette, J. J.: Impact of
631 an improved shortwave radiation scheme in the MAECHAM5 General Circulation Model, *Atmos.*
632 *Chem. Phys.*, 7(10), 2503–2515, doi:10.5194/acp-7-2503-2007, 2007.
- 633 Christoudias, T., Pozzer, A. and Lelieveld, J.: Influence of the North Atlantic Oscillation on air
634 pollution transport, *Atmos. Chem. Phys.*, 12(2), 869–877, doi:10.5194/acp-12-869-2012, 2012.
- 635 Claassen, H. C. and Halm, D. R.: A possible deficiency in estimates of wet deposition obtained
636 from data generated by the NADP/NTN network, *Atmos. Environ.*, 29(3), 437–448,
637 doi:10.1016/1352-2310(94)00182-K, 1995.
- 638 Cofala, J., Amann, M., Klimont, Z., Kupiainen, K. and Höglund-Isaksson, L.: Scenarios of
639 global anthropogenic emissions of air pollutants and methane until 2030, *Atmos. Environ.*, 41(38),
640 8486–8499, doi:10.1016/j.atmosenv.2007.07.010, 2007.
- 641 Croci-Maspoli, M., Schwierz, C. and Davies, H. C.: Atmospheric blocking: space-time links to
642 the NAO and PNA, *Clim. Dyn.*, 29(7-8), 713–725, doi:10.1007/s00382-007-0259-4, 2007.
- 643 Davini, P. and Cagnazzo, C.: On the misinterpretation of the North Atlantic Oscillation in
644 CMIP5 models, *Clim. Dyn.*, 43(5-6), 1497–1511, doi:10.1007/s00382-013-1970-y, 2013.
- 645 Davini, P., Cagnazzo, C., Gualdi, S. and Navarra, A.: Bidimensional Diagnostics, Variability,
646 and Trends of Northern Hemisphere Blocking, *J. Clim.*, 25(19), 6496–6509, doi:10.1175/JCLI-D-
647 12-00032.1, 2012.
- 648 Eckhardt, S., Stohl, A., Beirle, S., Spichtinger, N., James, P., Forster, C., Junker, C., Wagner,
649 T., Platt, U. and Jennings, S. G.: The North Atlantic Oscillation controls air pollution transport to
650 the Arctic, *Atmos. Chem. Phys.*, 3(5), 1769–1778, doi:10.5194/acp-3-1769-2003, 2003.
- 651 EEA: European Environment Agency: Air quality in Europe, Tech. rep., Luxembourg,
652 Publications Office of the European Union., 2013.
- 653 Feichter, J., Kjellström, E., Rodhe, H., Dentener, F., Lelieveld, J. and Roelofs, G.-J.:
654 Simulation of the tropospheric sulfur cycle in a global climate model, *Atmos. Environ.*, 30(10-11),
655 1693–1707, doi:10.1016/1352-2310(95)00394-0, 1996.
- 656 Feichter, J., Roeckner, E., Lohmann, U. and Liepert, B.: Nonlinear Aspects of the Climate
657 Response to Greenhouse Gas and Aerosol Forcing, *J. Clim.*, 17(12), 2384–2398, doi:10.1175/1520-
658 0442(2004)017<2384:NAOTCR>2.0.CO;2, 2004.
- 659 Fiore, A. M., Naik, V., Spracklen, D. V., Steiner, A., Unger, N., Prather, M., Bergmann, D.,
660 Cameron-Smith, P. J., Cionni, I., Collins, W. J., Dalsøren, S., Eyring, V., Folberth, G. A., Ginoux,
661 P., Horowitz, L. W., Josse, B., Lamarque, J.-F., MacKenzie, I. A., Nagashima, T., O'Connor, F. M.,
662 Righi, M., Rumbold, S. T., Shindell, D. T., Skeie, R. B., Sudo, K., Szopa, S., Takemura, T. and
663 Zeng, G.: Global air quality and climate., *Chem. Soc. Rev.*, 41(19), 6663–83,
664 doi:10.1039/c2cs35095e, 2012.
- 665 Fischer-Bruns, I., Banse, D. F. and Feichter, J.: Future impact of anthropogenic sulfate aerosol
666 on North Atlantic climate, *Clim. Dyn.*, 32(4), 511–524, doi:10.1007/s00382-008-0458-7, 2008.
- 667 Gillett, N. P. and Fyfe, J. C.: Annular mode changes in the CMIP5 simulations, *Geophys. Res.*
668 *Lett.*, 40(6), 1189–1193, doi:10.1002/grl.50249, 2013.
- 669 Gleckler, P. J., Taylor, K. E. and Doutriaux, C.: Performance metrics for climate models, *J.*
670 *Geophys. Res.*, 113(D6), D06104, doi:10.1029/2007JD008972, 2008.
- 671 Hilmer, M. and Jung, T.: Evidence for a recent change in the link between the North Atlantic
672 Oscillation and Arctic Sea ice export, *Geophys. Res. Lett.*, 27(7), 989–992,
673 doi:10.1029/1999GL010944, 2000.
- 674 Hoerling, M. P., Hurrell, J. W. and Xu, T.: Tropical origins for recent North Atlantic climate
675 change., *Science*, 292(5514), 90–2, doi:10.1126/science.1058582, 2001.

- 676 Hori, M. E., Nohara, D. and Tanaka, H. L.: Influence of Arctic Oscillation towards the Northern
677 Hemisphere Surface Temperature Variability under the Global Warming Scenario, *J. Meteorol. Soc.*
678 *Japan*, 85(6), 847–859, doi:10.2151/jmsj.85.847, 2007.
- 679 Horton, D. E., Skinner, C. B., Singh, D. and Diffenbaugh, N. S.: Occurrence and persistence of
680 future atmospheric stagnation events, *Nat. Clim. Chang.*, 4(8), 698–703, doi:10.1038/nclimate2272,
681 2014.
- 682 Hu, Z.-Z. and Wu, Z.: The intensification and shift of the annual North Atlantic Oscillation in a
683 global warming scenario simulation, *Tellus A*, 56(2), 112–124, doi:10.1111/j.1600-
684 0870.2004.00050.x, 2004.
- 685 Hurrell, J. W.: Decadal trends in the north atlantic oscillation: regional temperatures and
686 precipitation., *Science*, 269(5224), 676–9, doi:10.1126/science.269.5224.676, 1995.
- 687 IMAGE-team: The IMAGE 2.2 implementation of the SRES scenarios. A comprehensive
688 analysis of emissions, climate change and impacts in the 21st century, CD-ROM Publ. Bilthoven,
689 Natl. Inst. Public Heal. Environ., 2001.
- 690 IPCC: Climate Change 2013: The Physical Science Basis. Contribution of Working Group I to
691 the Fifth Assessment Report of the Intergovernmental Panel on Climate Change, edited by T. F.
692 Stocker, D. Qin, G.-K. Plattner, M. Tignor, S. K. Allen, J. Boschung, A. Nauels, Y. Xia, V. Bex,
693 and P. M. Midgley, Cambridge University Press, Cambridge, United Kingdom and New York, NY,
694 USA., 2013.
- 695 Jacob, D. J. and Winner, D. A.: Effect of Climate Change on Air Quality, *Atmos. Environ.*, 43,
696 51–63 [online] Available from: <http://dash.harvard.edu/handle/1/3553961> (Accessed 9 October
697 2014), 2009.
- 698 Karpechko, A. Y.: Uncertainties in future climate attributable to uncertainties in future
699 Northern Annular Mode trend, *Geophys. Res. Lett.*, 37(20), L20702, doi:10.1029/2010GL044717,
700 2010.
- 701 Kloster, S., Dentener, F., Feichter, J., Raes, F., van Aardenne, J., Roeckner, E., Lohmann, U.,
702 Stier, P. and Swart, R.: Influence of future air pollution mitigation strategies on total aerosol
703 radiative forcing, *Atmos. Chem. Phys.*, 8(21), 6405–6437, doi:10.5194/acp-8-6405-2008, 2008.
- 704 Kloster, S., Dentener, F., Feichter, J., Raes, F., Lohmann, U., Roeckner, E. and Fischer-Bruns,
705 I.: A GCM study of future climate response to aerosol pollution reductions, *Clim. Dyn.*, 34(7-8),
706 1177–1194, doi:10.1007/s00382-009-0573-0, 2009.
- 707 Kuzmina, S. I.: The North Atlantic Oscillation and greenhouse-gas forcing, *Geophys. Res.*
708 *Lett.*, 32(4), L04703, doi:10.1029/2004GL021064, 2005.
- 709 Lim, G. H. and Wallace, J. M.: Structure and Evolution of Baroclinic Waves as Inferred from
710 Regression Analysis, *J. Atmos. Sci.*, 48(15), 1718–1732, doi:10.1175/1520-
711 0469(1991)048<1718:SAEOWB>2.0.CO;2, 1991.
- 712 Lohmann, U., Stier, P., Hoose, C., Ferrachat, S., Kloster, S., Roeckner, E. and Zhang, J.: Cloud
713 microphysics and aerosol indirect effects in the global climate model ECHAM5-HAM, *Atmos.*
714 *Chem. Phys.*, 7(13), 3425–3446, doi:10.5194/acp-7-3425-2007, 2007.
- 715 Müller, W. A. and Roeckner, E.: ENSO teleconnections in projections of future climate in
716 ECHAM5/MPI-OM, *Clim. Dyn.*, 31(5), 533–549, doi:10.1007/s00382-007-0357-3, 2008.
- 717 Nakicenovic, N. and ...: Special Report on Emissions Scenarios: A Special Report of Working
718 Group III of the Intergovernmental Panel on Climate Change, Cambridge University Press,
719 Cambridge, UK., 2000.
- 720 Nazarenko, L. and Menon, S.: Varying trends in surface energy fluxes and associated climate
721 between 1960 and 2002 based on transient climate simulations, *Geophys. Res. Lett.*, 32(22),
722 L22704, doi:10.1029/2005GL024089, 2005.

- 723 Omrani, N.-E., Keenlyside, N. S., Bader, J. and Manzini, E.: Stratosphere key for wintertime
724 atmospheric response to warm Atlantic decadal conditions, *Clim. Dyn.*, 42(3-4), 649–663,
725 doi:10.1007/s00382-013-1860-3, 2013.
- 726 Pausata, F. S. R., Li, C., Wettstein, J. J., Nisancioglu, K. H. and Battisti, D. S.: Changes in
727 atmospheric variability in a glacial climate and the impacts on proxy data: a model intercomparison,
728 *Clim. Past*, 5, 489–502, doi:doi:10.5194/cp-5-489-2009, 2009.
- 729 Pausata, F. S. R., Pozzoli, L., Dingenen, R. Van, Vignati, E., Cavalli, F. and Dentener, F. J.:
730 Impacts of changes in North Atlantic atmospheric circulation on particulate matter and human
731 health in Europe, *Geophys. Res. Lett.*, 40(15), 4074–4080, doi:10.1002/grl.50720, 2013.
- 732 Pausata, F. S. R., Pozzoli, L., Vignati, E. and Dentener, F. J.: North Atlantic Oscillation and
733 tropospheric ozone variability in Europe: model analysis and measurements intercomparison,
734 *Atmos. Chem. Phys.*, 12(14), 6357–6376, doi:10.5194/acp-12-6357-2012, 2012.
- 735 Pelly, J. L. and Hoskins, B. J.: A New Perspective on Blocking, *J. Atmos. Sci.*, 60(5), 743–755,
736 doi:10.1175/1520-0469(2003)060<0743:ANPOB>2.0.CO;2, 2003.
- 737 Peterson, K. A., Lu, J. and Greatbatch, R. J.: Evidence of nonlinear dynamics in the eastward
738 shift of the NAO, *Geophys. Res. Lett.*, 30(2), 1030, doi:10.1029/2002GL015585, 2003.
- 739 Pham, M.: Changes in atmospheric sulfur burdens and concentrations and resulting radiative
740 forcings under IPCC SRES emission scenarios for 1990–2100, *J. Geophys. Res.*, 110(D6), D06112,
741 doi:10.1029/2004JD005125, 2005.
- 742 Rex, D. F.: Blocking Action in the Middle Troposphere and its Effect upon Regional Climate,
743 *Tellus*, 2(3), 196–211, doi:10.1111/j.2153-3490.1950.tb00331.x, 1950.
- 744 Riahi, K. and Roehrl, R. A.: Greenhouse Gas Emissions in a Dynamics-as-Usual Scenario of
745 Economic and Energy Development, *Technol. Forecast. Soc. Change*, 63(2-3), 175–205,
746 doi:10.1016/S0040-1625(99)00111-0, 2000.
- 747 Roeckner, E., Bäuml, G., Bonaventura, L., Brokopf, R., Esch, M., Giorgetta, M., Hagemann, S.,
748 Kirchner, I., Kornblueh, L., Manzini, E., Rhodin, A., Schlese, U., Schulzweida, U. and Tompkins,
749 A.: The atmospheric general circulation model ECHAM5—Part I: Model description, *Tech. Rep.*
750 349, Max-Planck-Institut für Meteorologie, Hamburg, Germany., 2003.
- 751 Roeckner, E., Bengtsson, L., Feichter, J., Lelieveld, J. and Rodhe, H.: Transient Climate
752 Change Simulations with a Coupled Atmosphere–Ocean GCM Including the Tropospheric Sulfur
753 Cycle, *J. Clim.*, 12(10), 3004–3032, doi:10.1175/1520-0442(1999)012<3004:TCCSWA>2.0.CO;2,
754 1999.
- 755 Roeckner, E., Siebert, T. and Feichter, J.: Climatic response to anthropogenic sulfate forcing
756 simulated with a general circulation model, in *Aerosol Forcing of Climate*, edited by R. J. Charlson
757 and J. Heintzenberg, pp. 349–362, John Wiley & Sons Ltd., Chichester., 1995.
- 758 Roelofs, G.-J., Lelieveld, J. and Ganzeveld, L.: Simulation of global sulfate distribution and the
759 influence on effective cloud drop radii with a coupled photochemistry sulfur cycle model, *Tellus B*,
760 50(3), doi:10.3402/tellusb.v50i3.16098, 1998.
- 761 Rosenblatt, M.: Remarks on Some Nonparametric Estimates of a Density Function, *Ann. Math.*
762 *Stat.*, 27(3), 832–837, 1956.
- 763 Scaife, A. A., Knight, J. R., Vallis, G. K. and Folland, C. K.: A stratospheric influence on the
764 winter NAO and North Atlantic surface climate, *Geophys. Res. Lett.*, 32(18), L18715,
765 doi:10.1029/2005GL023226, 2005.
- 766 Shindell, D., Kuylenstierna, J. C. I., Vignati, E., van Dingenen, R., Amann, M., Klimont, Z.,
767 Anenberg, S. C., Muller, N., Janssens-Maenhout, G., Raes, F., Schwartz, J., Faluvegi, G., Pozzoli,
768 L., Kupiainen, K., Höglund-Isaksson, L., Emberson, L., Streets, D., Ramanathan, V., Hicks, K.,
769 Oanh, N. T. K., Milly, G., Williams, M., Demkine, V. and Fowler, D.: Simultaneously mitigating

- 770 near-term climate change and improving human health and food security., *Science*, 335(6065), 183–
771 9, doi:10.1126/science.1210026, 2012.
- 772 Sillmann, J., Pozzoli, L., Vignati, E., Kloster, S. and Feichter, J.: Aerosol effect on climate
773 extremes in Europe under different future scenarios, *Geophys. Res. Lett.*, 40(10), 2290–2295,
774 doi:10.1002/grl.50459, 2013.
- 775 Stephenson, D. B., Pavan, V., Collins, M., Junge, M. M. and Quadrelli, R.: North Atlantic
776 Oscillation response to transient greenhouse gas forcing and the impact on European winter climate:
777 a CMIP2 multi-model assessment, *Clim. Dyn.*, 27(4), 401–420, doi:10.1007/s00382-006-0140-x,
778 2006.
- 779 Stier, P., Feichter, J., Kinne, S., Kloster, S., Vignati, E., Wilson, J., Ganzeveld, L., Tegen, I.,
780 Werner, M., Balkanski, Y., Schulz, M., Boucher, O., Minikin, A. and Petzold, A.: The aerosol-
781 climate model ECHAM5-HAM, *Atmos. Chem. Phys.*, 5(4), 1125–1156, doi:10.5194/acp-5-1125-
782 2005, 2005.
- 783 Sundquist, H., Berge, E. and Kristjansson, J. E.: Condensation and cloud parameterization
784 studies with a mesoscale numerical prediction model, *Mon. Wea. Rev.*, 117, 1641–1657, 1989.
- 785 Textor, C., Schulz, M., Guibert, S., Kinne, S., Balkanski, Y., Bauer, S., Berntsen, T., Berglen,
786 T., Boucher, O., Chin, M., Dentener, F., Diehl, T., Feichter, J., Fillmore, D., Ginoux, P., Gong, S.,
787 Grini, A., Hendricks, J., Horowitz, L., Huang, P., Isaksen, I. S. A., Iversen, T., Kloster, S., Koch,
788 D., Kirkevåg, A., Kristjansson, J. E., Krol, M., Lauer, A., Lamarque, J. F., Liu, X., Montanaro, V.,
789 Myhre, G., Penner, J. E., Pitari, G., Reddy, M. S., Seland, Ø., Stier, P., Takemura, T. and Tie, X.:
790 The effect of harmonized emissions on aerosol properties in global models – an AeroCom
791 experiment, *Atmos. Chem. Phys.*, 7(17), 4489–4501, doi:10.5194/acp-7-4489-2007, 2007.
- 792 Tibaldi, S. and Molteni, F.: On the operational predictability of blocking, *Tellus A*, 42(3), 343–
793 365, doi:10.1034/j.1600-0870.1990.t01-2-00003.x, 1990.
- 794 Toon, O. B. and Ackerman, T. P.: Algorithms for the calculation of scattering by stratified
795 spheres., *Appl. Opt.*, 20(20), 3657–60, doi:10.1364/AO.20.003657, 1981.
- 796 Twomey, S.: The Influence of Pollution on the Shortwave Albedo of Clouds, *J. Atmos. Sci.*,
797 34(7), 1149–1152, 1977.
- 798 Vignati, E.: M7: An efficient size-resolved aerosol microphysics module for large-scale aerosol
799 transport models, *J. Geophys. Res.*, 109(D22), D22202, doi:10.1029/2003JD004485, 2004.
- 800 Walker, G. T. and Bliss, E. W.: World weather V, *Mem. R. Meteorol. Soc.*, 4, 53 – 84, 1932.
- 801 WHO: Review of evidence on health aspects of air pollution – REVIHAAP Project. First
802 results., Tech. rep., Copenhagen, World Health Organization., 2013.
- 803 Woollings, T., Hoskins, B., Blackburn, M. and Berrisford, P.: A New Rossby Wave-Breaking
804 Interpretation of the North Atlantic Oscillation, *J. Atmos. Sci.*, 65(2), 609–626,
805 doi:10.1175/2007JAS2347.1, 2008.
- 806 Yao, Y. and Luo, D.: Relationship between zonal position of the North Atlantic Oscillation and
807 Euro-Atlantic blocking events and its possible effect on the weather over Europe, *Sci. China Earth
808 Sci.*, doi:10.1007/s11430-014-4949-6, 2014.
- 809 Yiou, P. and Nogaj, M.: Extreme climatic events and weather regimes over the North Atlantic:
810 When and where?, *Geophys. Res. Lett.*, 31(7), L07202, doi:10.1029/2003GL019119, 2004.
- 811
812
813
814
815

816 **Table 1:** ECHAM5-HAM experiment design and number of years simulated for each experiment.
 817 The original denomination used by Kloster et al. (2009) is shown in the last column.

Experiment	GHG	Aerosol emissions	Years of simulation	Original names
2000	2000	2000	60	CONTROL
2030	2030	2030	30	GHG+AE
2030GHG	2030	2000	30	GHG
2030AER	2000	2030	30	AE

818
 819 **Table 2:** Skewness values for the PM distributions of the four selected regions for each
 820 experiment. For each region and experiment, changes relative to all the other experiments are
 821 significant at the 95% confidence level, except for 2030-2030AER in Western Mediterranean.

	Western Mediterranean	Eastern Mediterranean	Central Europe	Eastern Europe
2000	0.26	0.83	1.44	1.70
2030	1.02	0.95	0.66	1.18
2030GHG	0.48	1.26	1.18	1.08
2030AER	1.05	1.17	0.94	1.03

822
 823 **Table 3:** Percentiles of PM anomaly distributions for the WM and CE regions in the 2000
 824 experiment and their relative changes (in %) for the 2030 simulation compared to 2000 values.

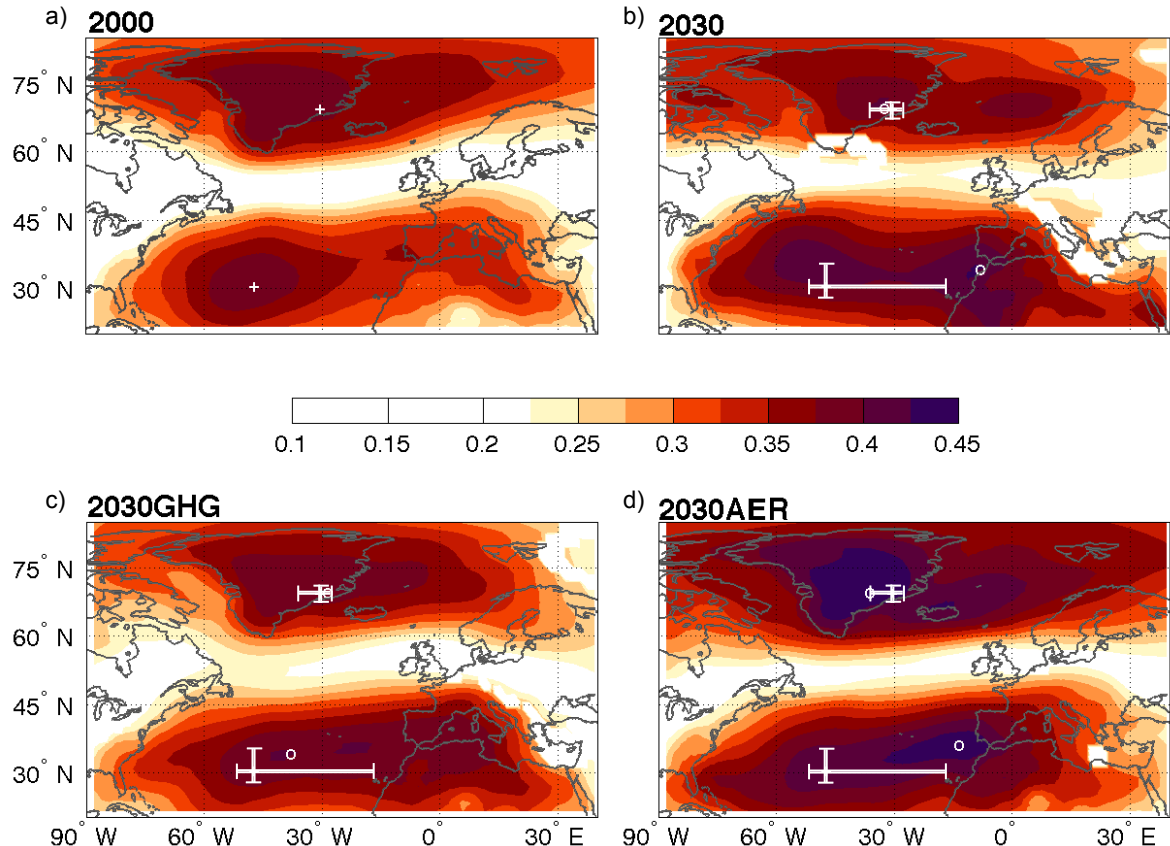
Region	Experiment	Percentile				
		5 th	25 th	50 th	75 th	95 th
Western Mediterranean	2000	0.49	0.73	1.01	1.25	1.57
	2030	+8%	+1%	-9%	-7%	+4%
Central Europe	2000	0.65	0.80	0.94	1.13	1.48
	2030	-14%	-3%	+2%	+2%	+7%

825
 826 **Table 4:** Qualitative contributions (small (+), medium (++) , high (+++)) of 2030 GHG and AER to
 827 changes in the NAO phase, SCoA location and blocking event frequency. For the blocking events
 828 the direction of the increased frequency is also shown. The contributions significant at 95%
 829 confidence level are shown in bold

	Impact on NAO	Impact on SCoA	Impact on Blocking Events
2030GHG	++	+	North ++ East +
2030AER	+	+++	North ++ East +++
2030 (GHG+AER)	+++	+++	North +++ East +++

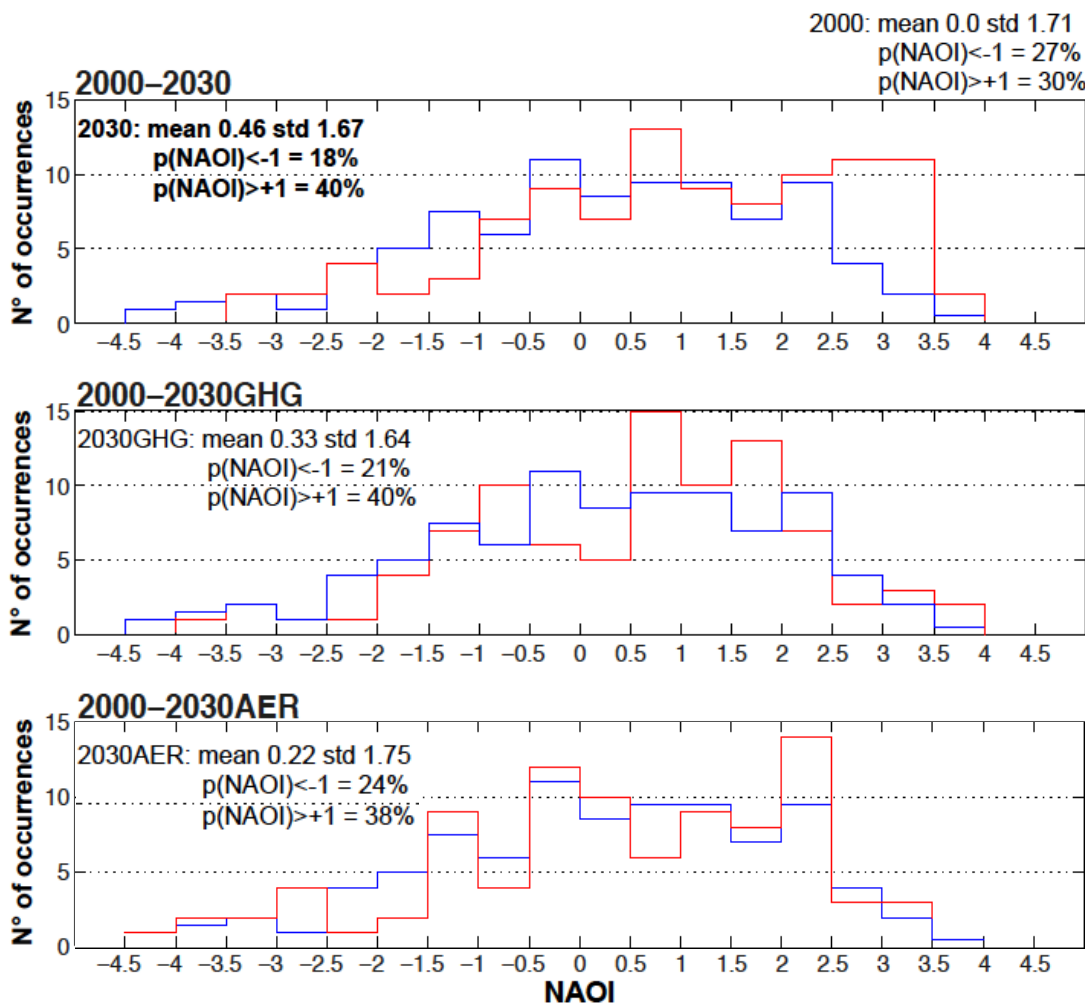
830

831

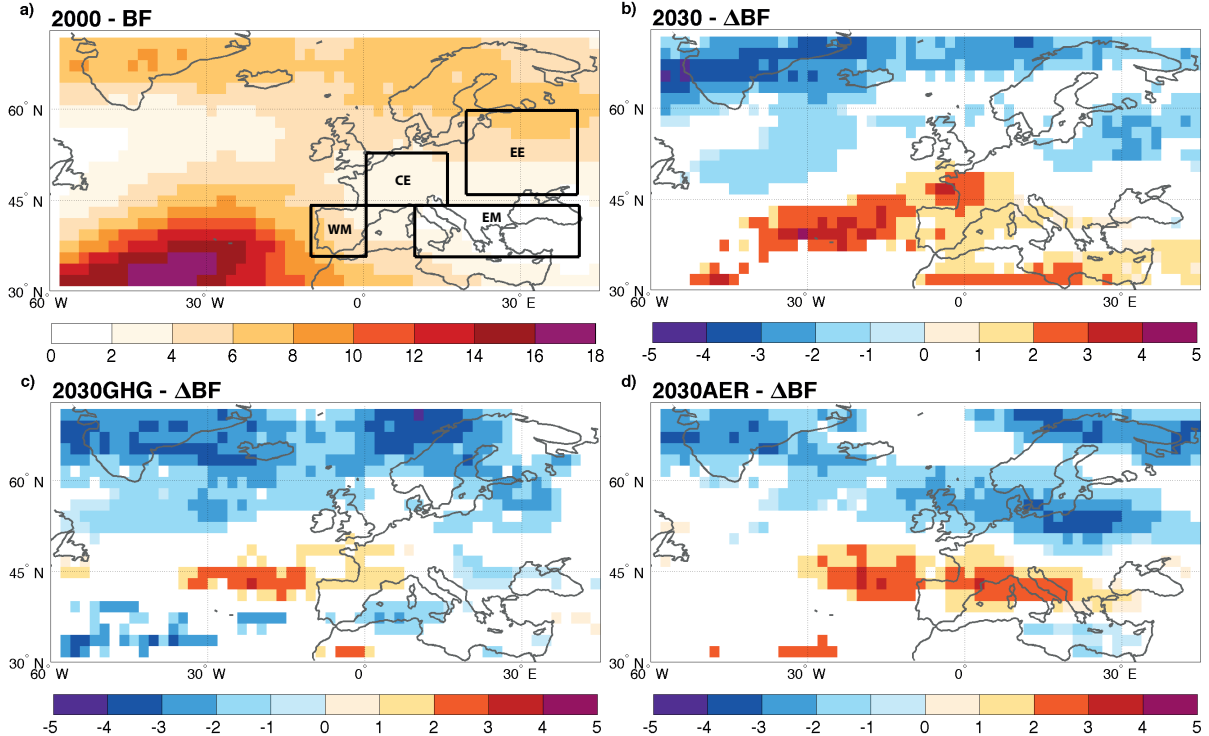


834
835
836
837
838
839
840
841

Fig. 1: Sea Level Pressure coherence index maps of the North Atlantic sector for the 2000 (a) and 2030 (b) simulations and the two sensitivity studies (c and d) in winter (DJF). The SLP centres of action (COAs) for the control run and for the 2030 simulations are shown by white crosses and white circles, respectively. The bars delimit the range between the 10th and 90th percentile of the CI maxima in the 2000 simulations. Only areas in which the difference between the 2000 control pattern and the sensitivity simulation is significant at the 95% confidence level and CI values are greater than 0.225 are shaded. The choice of shading only CI values greater than 0.225 is arbitrary.



853 **Fig. 2:** Frequency distributions of the winter (DJF) NAOI for the 2000 control simulation (blue,
 854 all panels), 2030 (red, upper panel), 2030GHG (red, central panel) and 2030AER (red, lower
 855 panel). Numbers show the NAOI mean value, the standard deviation (std) and the probability of
 856 having a NAOI greater than +1 ($p(\text{NAOI})>+1$) or smaller than -1 ($p(\text{NAOI})<-1$). Values of the
 857 simulations having a NAOI mean significantly different from 2000 control mean at 95%
 858 confidence level are shown in bold. The 2000s mean NAO is by definition equal to 0 and the
 859 number of occurrences has been normalized to 30 years for a direct comparison with the other
 860 simulations.

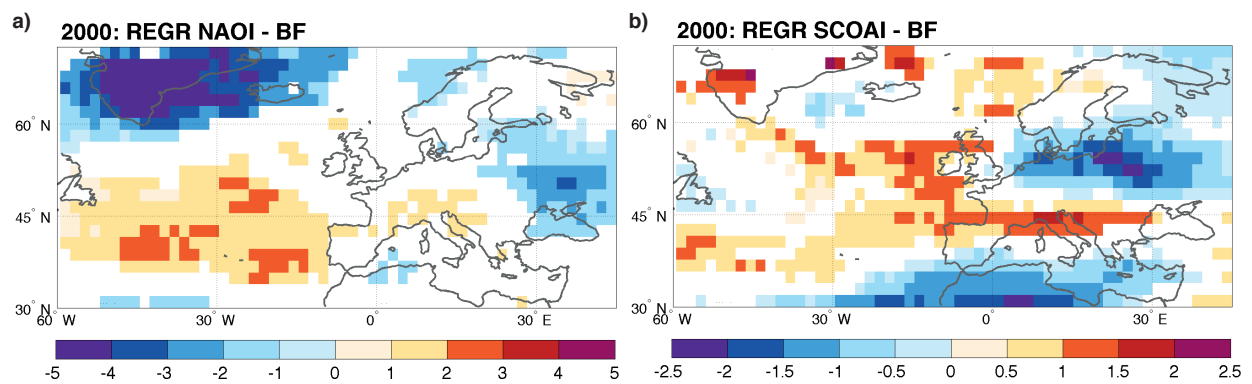


864

865 **Fig. 3:** Blocking frequency (in % of days in which a blocking event occurs at a given grid box)
866 over the Atlantic sector for the 2000 simulation (a); changes in blocking frequency compared to
867 the 2000 simulation for 2030 (b), 2030GHG (c) and 2030AER (d) simulations in winter (DJF).
868 Only areas in which the difference between the 2000 control and the sensitivity simulation is
869 significant at 95% confidence level are shaded (in white non-significant areas). In panel (a) we
870 have highlighted the regions discussed in Section 3.3 and Table 2.

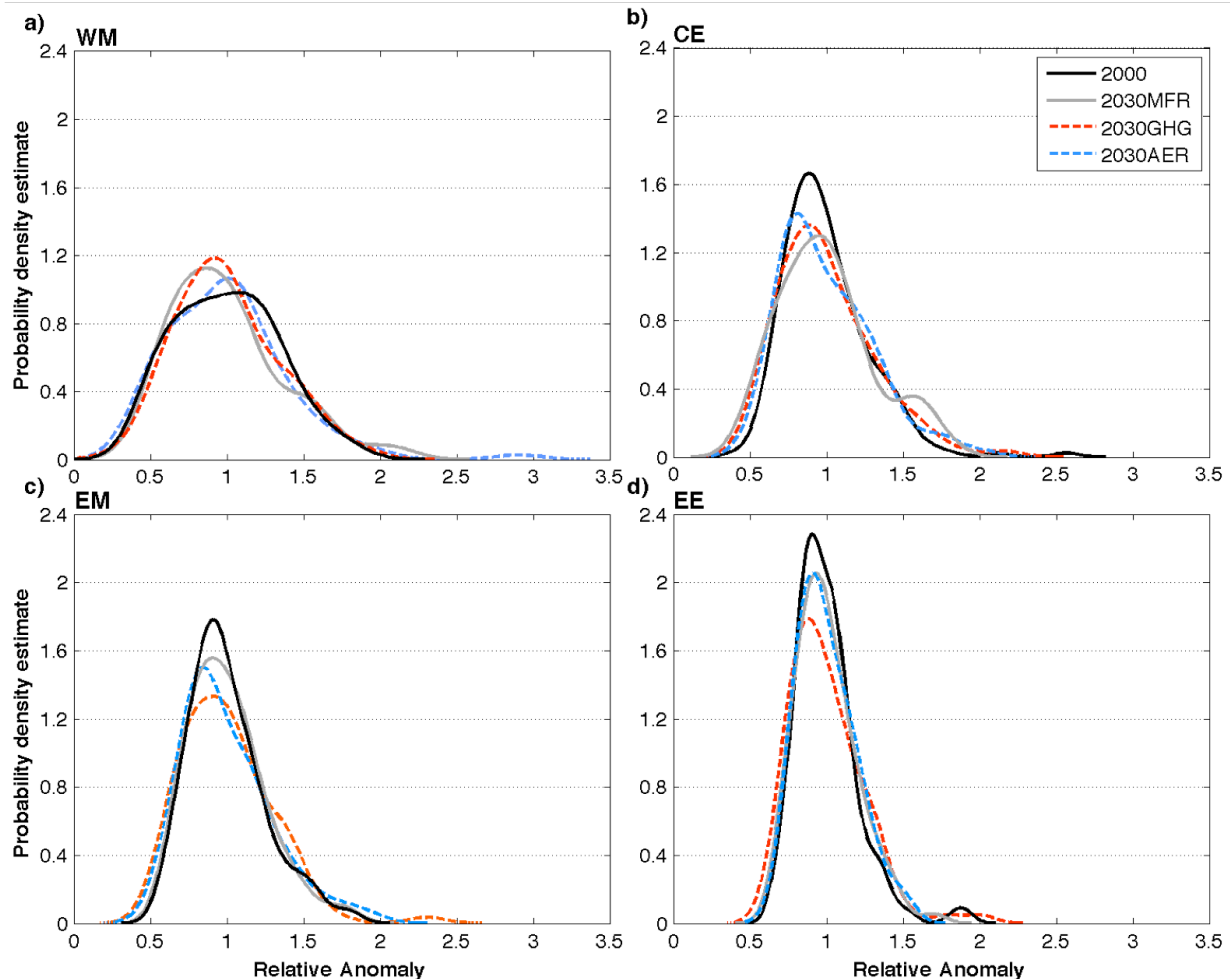
871

872



873
874 **Fig. 4:** Blocking frequency anomalies (in % of days in which a blocking event occur at a given
875 grid box) per unit of NAOI index (NAOI, a) and SCOAI index (SCOAI, b) standard deviation.
876 The anomalies are calculated using a one-point regression analysis (see Appendix B). Only
877 differences significant at the 95% confidence level are shown (based on the correlation
878 significance between NAOI/SCOAI and blocking frequency). Note that the two panels use
879 different colour-scales.

880
881
882
883



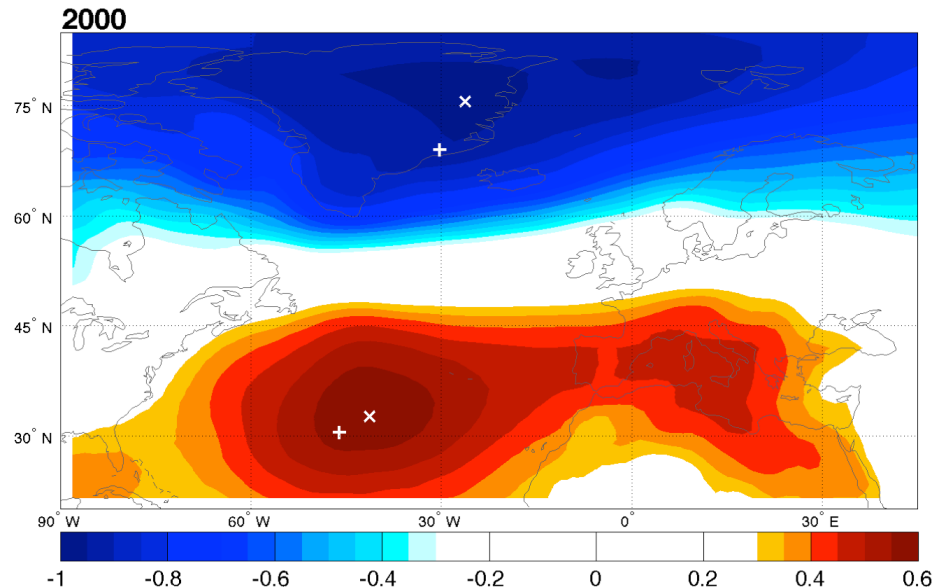
884

885 **Fig. 5:** Probability density estimate (PDE) of PM relative anomalies for each region (Western
886 and Eastern Mediterranean, Central and Eastern Europe) and for each experiment. Relative
887 anomalies are computed as the ratio between winter (DJF) monthly timeseries and the winter
888 (DJF) climatology of each experiment and region. The probability density estimates are based on
889 a normal kernel function, which provides non-parametric PDEs for random variables
890 (Rosenblatt, 1956). The probability for a given relative anomaly to occur is obtained by
891 integrating the PDE in dx .

892
893
894
895

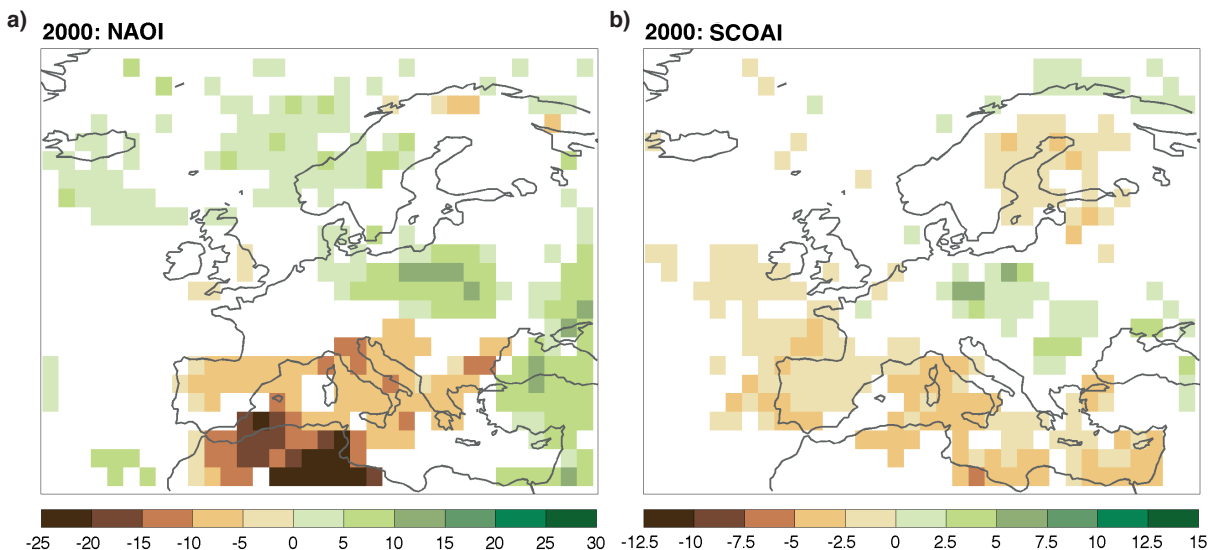
896

897



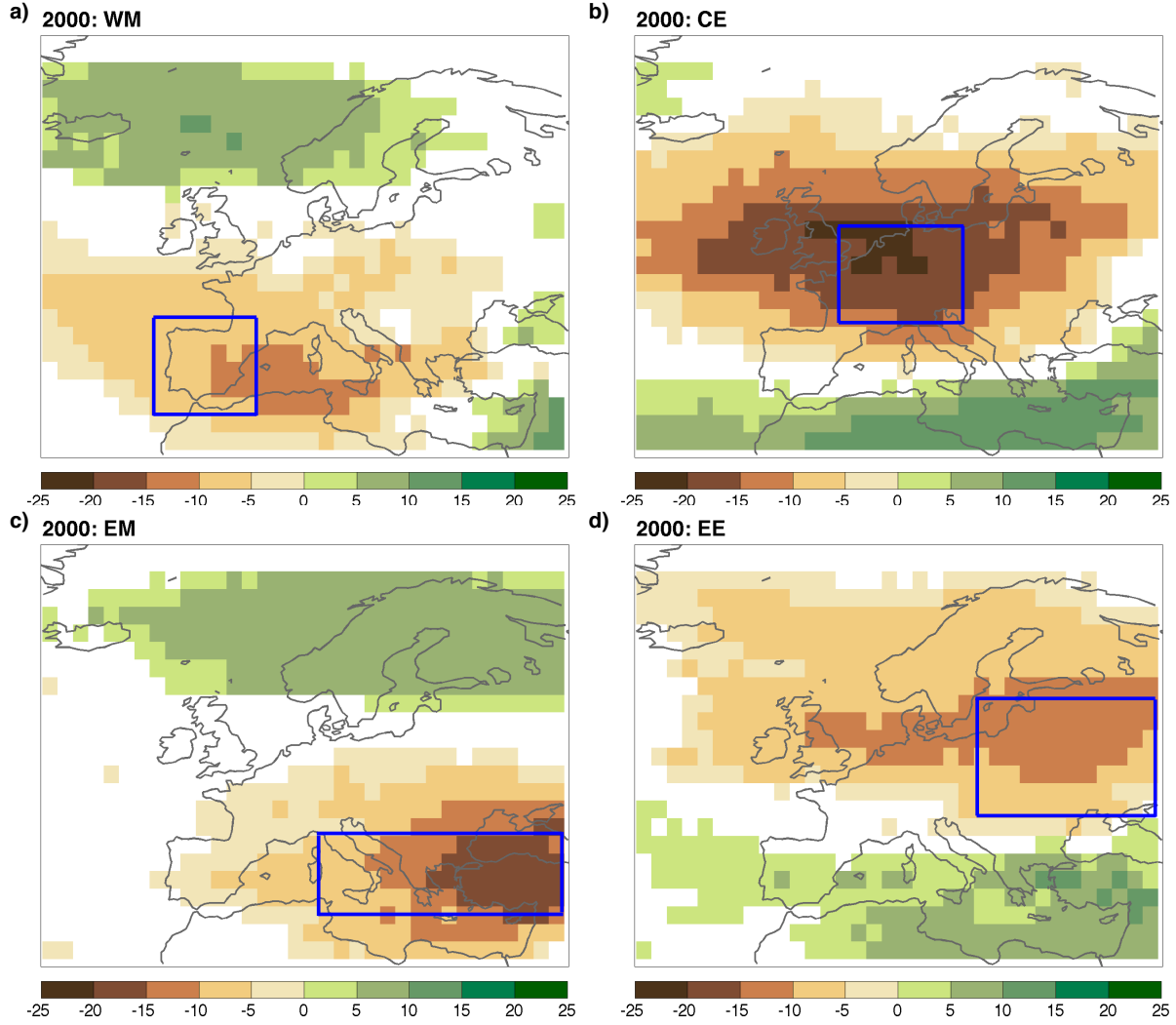
898

Figure A1: Correlations between North Atlantic winter SLP (December to February) and the PC1 of SLP. The markers indicate the maxima in CI (+ sign) and in the SLP/PC1 (x sign) correlations.
900
901



902

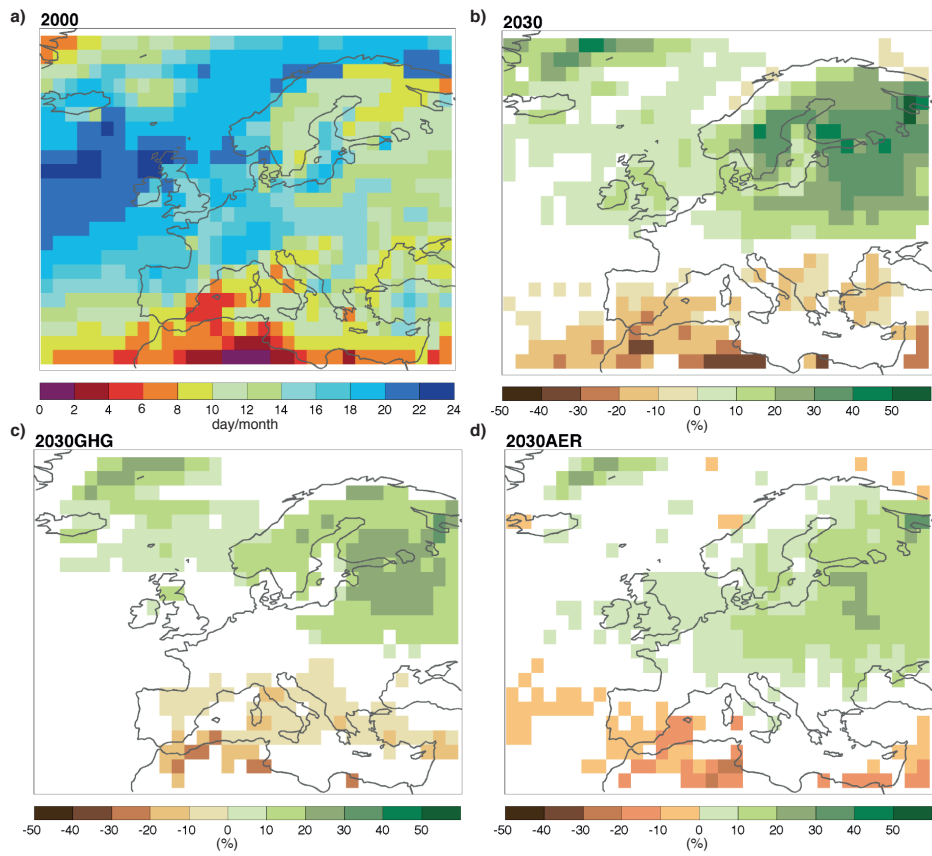
Fig. B1: Rainy day anomalies (in %) per unit of NAOI (a) and CI time-series (b) standard deviation. The CI time-series has been constructed as described in Appendix B. The anomalies are calculated using a one-point regression analysis. Only differences significant at the 95% confidence level are shown. Note that the two panels use different colour-scales.
904
905
906
907
. .
908
909



910

911 **Fig. B2:** The values at each gridpoint show the composite anomaly in rainy days (in %) in the
912 selected domain – a) WM, b) CE, c) EM, d) EE) – while said gridpoint is blocked relative to
913 rainy days in the selected domain while the gridpoint is unblocked. The composite is taken by
914 averaging the rainy day anomaly maps obtained for each gridbox within the selected domain.
915 For example, in panel a) (WM) the positive values over southern Norway indicate that, when
916 there is a blocking event there, rainy days over the WM increase by about 10% compared to the
917 case with no blocking over southern Norway. On the other hand, blocking events west and over
918 the WM lead to 10-15% precipitation anomalies relative to the case with no blocking events over
919 the same regions. The regional domains analysed in each panel are marked by the blue
920 rectangles.

921



922

923 **Fig. C1:** Average number of rainy day per month during winter (DJF) in the 2000 simulation (a).
 924 Percent changes in the average number of rainy days per month for 2030 (b), 2030GHG (c), and
 925 2030AER (d) simulations during winter. Only differences significant at the 95% confidence level
 926 are shown.

927